ISSN 2079-1704. Хімія, фізика та технологія поверхні. 2022. Т. 13. № 2. С. 127-149

PACS:61.43.Gt; 68.03.-g; 68.43.-h; 81.40.Ef doi: 10.15407/hftp13.02.127

V.M. Gun'ko

TEXTURAL CHARACTERISTICS AND ORGANIZATION OF COMPOSITES WITH FUMED SILICAS AND HIGH-MOLECULAR WEIGHT COMPOUNDS

Chuiko Institute of Surface Chemistry of National Academy of Sciences of Ukraine
17 General Naumov Str., Kyiv, 03164, Ukraine, E-mail: vlad_gunko@ukr.net

Various composites with nanosilicas, as well as with other nanooxides, and polymers are of importance from a practical point of view. Detailed textural and morphological characterization, applied here to nanosilicas treated alone and in composites with a set of polymers (poly(vinyl pyrrolidone), poly(vinyl alcohol), poly(ethylene oxide), poly(ethylene glycol), polydimethylsiloxane, and polymethylsiloxane) and proteins (egg albumin, gelatin, and ossein), could be considered as a tool to evaluate the reorganization of hierarchical structures in composites from aggregates of nanoparticles, agglomerates of aggregates, to micro and visible particles. This analysis allows one to elucidate various changes in the porosity, accessible surface area, contributions of pores of different sizes and shapes and pore walls with silica or polymer/protein depending on a set of varied factors. Collected information could be used to forecast possible characteristics and properties of various composites with nanooxides. Among the factors affecting the properties and characteristics of the composites, a type, molecular weight, and content of a polymer and treatment conditions may play an important role. The presence of a large set of the factors makes difficult analysis of the composites using simplified approaches and methods. As a whole, selection of the composition and certain conditions of the composite preparation allows one to control all the textural characteristics of the final materials. For these purposes, the characteristics should be accurately estimated with minimum possible errors using well developed and adequate methods.

***Keywords**: fumed nanosilicas, polymers, proteins, composites, particulate morphology, textural characteristics*

INTRODUCTION

Fumed oxides are "soft" materials due to their hierarchical particular morphology and weak bonds between adjacent nonporous nanoparticles (NPNP). NPNP form loose aggregates (secondary structures typically < 1 μm in size, average coordination number of NPNP is between 2 and 3). The aggregates form very loose agglomerates (ternary structures > 1 μm), which form loose visible particles in the powders characterized by low bulk density ρ_b = 0.04–0.13 g/cm^3 [1–10]. The ρ_b value increases with decreasing specific surface area (SSA, S_{BET}) or increasing average NPNP sizes $d \approx 6/(\rho_0 S_{BET})$, where $\rho_0 \approx 2.2$ g/cm^3 is the true density of amorphous silica [8–10]. The low ρ_b value causes a great empty volume in the nanosilica powders $V_{em} = 1/\rho_b - 1/\rho_0$ up to 24.5 cm^3/g, which is much greater than the pore volume (V_p) value, determined from the nitrogen adsorption isotherms at relative pressure p/p_0 = 0.98–0.99. Voids between NPNP in the secondary and ternary structures provide textural porosity, mainly meso/macroporous. Typically, any treatment of nanosilicas causes increasing ρ_b value. The voids can be filled by adsorbed molecules, but nitrogen or other low-molecular weight probes can fill only a small part of V_{em} due to very weak interactions of adsorbate molecules with distant NPNP in agglomerates. Any low- or high-molecular weight adsorbate can change the organization of the secondary and ternary structures of fumed oxides because the bonds between neighboring NPNP are weak (non-covalent) and mainly caused by electrostatic and van-der-Waals forces [8–13]. Therefore, in sonicated aqueous suspensions, NPNP can be located alone or remain in certain aggregates that depends on several factors (concentration, pH, salinity, characteristics of fumed oxides, treatment conditions, *etc.*) [1–4, 8–14]. Wetting-suspending-adsorption-treating-drying results in strong reorganization of the secondary and ternary structures that affects the textural characteristics of dried residues [8]. The latter can be considered as nanocomposites, *e.g.*, in the case of polymer/nanooxide systems.

For composites with fumed oxides and polymers, there are such several hybrid systems as (i) polymers filled by NPNP (typically, the filler amount is < 10 wt. %); (ii) nanooxides

modified by adsorption or impregnation with polymers from solutions then dried (around monolayer coverage with 10–20 wt. % for linear polymers and up to 40–50 wt. % for globular proteins); (iii) nanooxides chemically modified by attached polymers (or fragments) up to monolayer coverage or higher; (iv) combination of two previous cases; (v) composites with close contents of polymers and fumed oxides (that are typically unstable) [1–4, 8, 9]. There are several methods of the composite preparation: (i) equilibrium adsorption of a polymer from a solution and separation of the residue; (ii) impregnation of a powder by a concentrated polymer solution; (iii) stirring of blends dry or with addition of a low amount (30–50 wt. %) of a solvent; (iv) precursor polymerization with the presence of solid particles; (v) formation of solid particles in a polymer or precursor solution; (vi) mixing of molten polymer with solid particles (*e.g.*, in 3D printing), *etc.* Many of these systems are of interest for different applications that determines limiting contents of nanooxides and polymers in the composites [15–32]. The composite organization depends not only on the contents of components but also on their characteristics, *e.g.*, surface composition of nanooxides, 2D- or 3D-structure, chemical composition of polymers, preparation routes and other conditions. Clearly, features of the polymer-polymer, polymer-NPNP, and NPNP-NPNP interactions play not only an important role in the properties and characteristics of the composites but also determine the reorganization of the hierarchical structures under any external action. Therefore, changes in the textural organization of polymer (or protein)/nanosilica composites prepared using various routes are here analyzed for different polymers: linear polydimethylsiloxane (PDMS) [33, 34], 3D polymethylsiloxane (PMS) [35–37], poly(vinyl pyrrolidone) (PVP) [38–43], poly(vinyl alcohol) (PVA) [43–45], poly(ethylene oxide) (PEO) [43, 46], and poly(ethylene glycol) (PEG) [43], and proteins: egg albumin, gelatin, and ossein [47–53], which are characterized by different adsorbate-adsorbate and adsorbate-NPNP interactions. Several samples of nanosilicas with the S_{BET} values from 232 to 378 m^2/g (for the pristine powders) are used to prepare various composites (105 samples in total).

As a whole, some properties of nanostructured materials could be negative, *e.g.*, easy dusting, too active surface sites generating charged and free radical particles, *etc*. [1–7, 10, 54–56]. To reduce the negative effects, several methods could be used, *e.g.*, controlled hydro-compaction (anti-dusting) [57] or mechano-chemical activation (MCA) under various conditions [58–62], surface adsorption or chemical modification by low- or high-molecular compounds (to change the surface nature), *etc*. [1–10, 23–53]. The surface sites, as well as the particle size distributions, can affect the toxic properties of nanostructured silicas or other nanooxides and composites [1–7, 50, 63]. However, certain modifications of fumed oxides can strongly change their textural and other characteristics that can affect the toxicity of the final materials. The aim of this study is to analyze the mentioned textural aspects upon interactions of fumed silicas with high-molecular compounds (polymers and proteins) prepared and treated under different conditions.

MATERIALS

Fumed silicas (A–300 and A–380, 99.8 % purity, S_{BET} = 232–378 m^2/g, Pilot plant of the Chuiko Institute of Surface Chemistry, Kalush, Ukraine) used as the initial materials were heated at 650–700 K for several hours to remove residual HCl and other adsorbed compounds [8–10, 57–62].

Poly(vinyl pyrrolidone), PVP (Biopharma, Kyiv, pharmaceutical purity) $(–CH_2CHR–)_n$, where R = NC_4H_6O, $n \approx 100$, molecular weight of 12600±2700, was used as received. Several series of PVP/nanosilica compositions were prepared using different conditions and treatment methods (Tables 1–3) described in detail elsewhere [38–43]. First (Table 1), the PVP solution was added to the aqueous suspension of silica (5 wt. %) MCA (a ball-mill of 1 dm^3, 30 porcelain balls at 2–3 cm in diameter, 60 rpm) treated during a few hours, or fumed silica powder was added to the PVP solution then agitated (1000 rpm) in a pseudo-liquid state reactor (PLSR) for several hours, then sonicated for 5–6 min and then dried. The concentration ratio $\gamma = C_{PVP}/C_{A\text{-}300}$ was between 0 and 1. The value $\gamma \leq 0.1$ corresponds to practically irreversible adsorption of PVP onto a silica surface, and evaluation of statistical monolayer coverage gives $\gamma \approx 0.17–0.19$. The PVP adsorption (Table 1) was determined spectrophotometrically [38–43].

Table 1. Characteristics of pristine powder and dried suspensions of fumed silica A-300 and silica/PVP

Sample	C_{PVP} (wt.%)	S_{BET} (m^2/g)	V_p (cm^3/g)	S_{nano} (m^2/g)	S_{meso} (m^2/g)	S_{macro} (m^2/g)	V_{nano} (cm^3/g)	V_{meso} (cm^3/g)	V_{macro} (cm^3/g)	$<R_V>$ (nm)	$<R_S>$ (nm)	Δw	c_{void}	c_{cyl}	c_{void}
[a]A–300	0	345	0.566	0.3	320	25	0.040	0.334	0.192	22.74	5.12	-0.389	0.100	0.880	0.120
[b]A–300	0	184	0.790	0	140	44	0.017	0.553	0.219	20.31	9.74	0.167	0.075	0.904	0.021
[b]A–300/PVP	5	173	1.055	23	133	17	0.010	0.751	0.294	20.77	11.16	0.026	0.057*	0.825*	0.118
[b]A–300/PVP	10	159	0.447	50	103	6	0.018	0.309	0.120	20.61	5.52	0.168	0.001*	0.655*	0.344
[a]A–300(1)	0	365	0.890	-	324	27	0.034	0.490	0.366	26.18	7.33	-0.290	0.224	0.691	0.085
A–300/PVP(2)	14.9	239	0.891	-	187	52	0.035	0.441	0.415	27.00	6.83	-0.006	0.068*	0.929*	0.003
A–300/PVP(3)	10.5	276	0.806	-	237	39	0.044	0.429	0.333	25.04	5.23	0.006	0.001*	0.826*	0.173
A–300/PVP(4)	10.5	279	1.218	-	208	71	0.040	0.508	0.699	29.36	7.67	-0.030	0.066*	0.867*	0.067
A–300/PVP(5)	10.5	278	0.953	-	228	49	0.027	0.439	0.487	28.74	7.07	-0.165	0.188*	0.510*	0.302

Note. [a]Pristine powder, [b]dried powders from solid residual of the aqueous suspensions; the *c* and **c* values are for silica (pore model with voids between NPNP) and PVP (voids and cylindrical pores with a surface covered by polymer) contributions. The V_{nano} and S_{nano} values were calculated by integration of the $f_V(R)$ and $f_S(R)$ function, respectively, at 0.35 nm <R< 1 nm, V_{meso} and S_{meso} at 1 nm <R< 25 nm, and V_{macro} and S_{macro} at 25 nm <R< 100 nm. Δw is the model error $\Delta w = [S_{BET} / \int_{R_{min}}^{R_{max}} f_S(R)dR] - 1$ for DFT VCV/SCR method. The values of $<R_V>$ and $<R_S>$ correspond to the first moments of the distribution functions $< R_X >= \int_{R_{min}}^{R_{max}} Rf_X(R)dR / \int_{R_{min}}^{R_{max}} f_X(R)dR$ with respect to the pore volume (X = V) and specific surface area (X = S)

Table 2. Characteristics of initial silica and PVP/silica differently treated

t_{MCA} (h)	γ	S_{BET} (m^2/g)	V_p (cm^3/g)	S_{meso} (m^2/g)	S_{macro} (m^2/g)	V_{nano} (cm^3/g)	V_{meso} (cm^3/g)	V_{macro} (cm^3/g)	$<R_V>$ (nm)	$<R_S>$ (nm)	Δw	c_{void}	c_{cyl}	c_{void}
9	0	311	0.732	276	35	0.019	0.407	0.306	27.16	7.52	-0.283	0.375	0.622	0.003
1	0	283	1.358	204	79	0.012	0.498	0.849	30.87	13.34	0.033	0.474	0.311	0.215
3	0	286	1.376	205	81	0.029	0.864	0.483	23.08	10.69	0.226	0.030	0.785	0.185
5	0	282	1.136	227	55	0.022	0.758	0.356	23.90	9.64	0.006	0.254	0.695	0.051
1	0.1	258	1.228	188	70	0.022	0.658	0.548	25.84	9.13	0.113	0.006*	0.728*	0.266
3	0.1	254	1.092	200	54	0.024	0.751	0.317	22.17	7.78	0.024	0*	0.799*	0.201
4	0.1	261	1.063	211	50	0.026	0.722	0.314	22.44	7.31	0.012	0.001*	0.787*	0.212
1	0.2	224	1.276	144	80	0.017	0.729	0.530	25.21	10.59	0.040	0.102*	0.832*	0.066
1	0.2	165	0.997	101	64	0.016	0.506	0.475	27.43	10.31	-0.045	0.004*	0.831*	0.165
1	0.2	166	0.848	123	43	0.011	0.537	0.301	25.63	9.46	0.096	0.246*	0.666*	0.088
3	0.2	163	0.637	134	29	0.017	0.553	0.067	14.20	6.56	0.099	0.037*	0.956*	0.007
5	0.2	166	0.553	144	22	0.012	0.462	0.080	15.19	5.73	-0.015	0*	0.764*	0.236

Note. Samples 2, 3, and 4 correspond to the MCA of dry A-300 for 1, 3, and 5 h, respectively. Samples 5, 6, and 7 are dry PVP/silica (γ = 0.1) after the MCA for 1, 3, and 5 h, respectively. Sample 8 is dry PVP/silica (γ= 0.2) after the MCA for 1 h. Sample 9 corresponds to Sample 8 dried after exposition in saturated vapor of water/ethanol (1:1) for 10 h. Samples 10, 11, and 12 correspond to dried powders with addition of 25% solution of PVP in a mixture of ethanol and water (1:1) giving γ= 0.2 (the ratio between silica + PVP and water + ethanol is 2:1) after the MCA for 1, 3, and 5 h, respectively; **c* values for PVP contribution at the pore walls

Table 3. Characteristics of initial silica and PVP/silica treated and dried

No	C_{PVP} (wt.%)	t_{act} (h)	H_2O/C_2H_5OH (wt.%)	S_{BET} (m^2/g)	V_p (cm^3/g)	S_{meso} (m^2/g)	S_{macro} (m^2/g)	V_{nano} (cm^3/g)	V_{meso} (cm^3/g)	V_{macro} (cm^3/g)	$<R_V>$ (nm)	$<R_S>$ (nm)	Δw	c_{void}	c_{cyl}	c_{void}
1	0	0	0/0	255	0.570	229	26	0.027	0.318	0.224	26.04	6.40	-0.306	0.019	0.574	0.407
2	0	1[a]	0/0	236	1.312	157	79	0.022	0.428	0.862	34.36	13.78	0.011	0.108	0.722	0.170
3	0	1[a]	30/0	234	0.921	187	47	0.028	0.597	0.296	23.49	8.63	-0.017	0.008	0.815	0.177
4	0	1[b]	30/0	239	0.999	189	50	0.019	0.530	0.449	28.84	10.45	-0.040	0.097	0.546	0.357
5	0	1[a]	0/30	243	0.764	205	38	0.017	0.363	0.384	29.53	9.15	-0.213	0.408	0.469	0.123
6	0	1[b]	0/30	253	0.684	220	33	0.026	0.336	0.322	29.05	7.70	-0.275	0.043	0.600	0.357
7	15	1[a]	30/0	164	0.877	116	48	0.016	0.587	0.274	22.53	8.72	-0.117	0.008*	0.928*	0.065
8	15	1[a]	0/30	172	0.879	120	52	0.015	0.493	0.371	25.67	9.33	0.012	0.003*	0.859*	0.138
9	15	3[b]	0/30	179	0.656	144	35	0.016	0.305	0.335	28.90	7.66	-0.123	0.223*	0.529*	0.248
10	15	0.5[b]	0/0	224	0.577	197	27	0.036	0.310	0.232	26.24	4.81	0.042	0.005*	0.844*	0.151
11	15	3[b]	0/0	177	0.755	133	44	0.019	0.275	0.461	31.78	8.51	-0.101	0*	0.676*	0.324
12	16	0.5[b]	0/0	218	0.569	192	26	0.027	0.305	0.237	27.48	5.19	0.214	0.058*	0.586*	0.356
13	16	9[b]	0/30	180	0.525	152	28	0.025	0.251	0.249	27.69	5.69	0.096	0.148*	0.819*	0.033
14	17.5	1[b]	0/0	235	0.755	199	36	0.033	0.340	0.382	31.84	5.97	0.021	0.002*	0.887*	0.111
15	17.5	1[b]	0/40	181	0.688	142	39	0.020	0.268	0.401	31.92	7.63	-0.179	0.006*	0.656*	0.338
16	17.5	3[b]	0/40	167	0.809	118	49	0.015	0.313	0.481	31.19	9.39	0.013	0.003*	0.665*	0.332
17	17.5	6[b]	0/40	170	0.909	113	57	0.015	0.405	0.489	29.87	10.01	0.067	0.011*	0.779*	0.210

Note. [a]MCA, [b]PLSR, *c values for PVP contribution

Table 4. Characteristics of A-300 alone and modified by PVA (15 wt.%)

Sample	S_{BET} (m^2/g)	V_p (cm^3/g)	S_{meso} (m^2/g)	S_{macro} (m^2/g)	V_{nano} (cm^3/g)	V_{meso} (cm^3/g)	V_{macro} (cm^3/g)	$<R_V>$ (nm)	$<R_S>$ (nm)	Δw	c_{void}	c_{cyl}	c_{void}
I	252	1.408	161	91	0.015	0.494	0.899	30.57	14.18	0.145	0.237	0.450	0.313
II	177	0.684	139	38	0.019	0.409	0.257	23.54	7.09	0.075	0.022*	0.700*	0.278
III	218	1.198	140	78	0.021	0.621	0.556	25.85	9.42	-0.012	0.170*	0.744*	0.086
IV	215	1.282	132	83	0.020	0.534	0.728	29.91	11.28	0.034	0*	0.903*	0.097
V	237	1.031	179	58	0.023	0.598	0.411	24.70	8.31	0.102	0*	0.741*	0.259
VI	230	0.782	191	39	0.029	0.485	0.268	22.61	6.40	0.057	0*	0.820*	0.180
VII	247	1.568	145	102	0.013	0.683	0.872	27.92	14.90	0.357	0.030	0.435	0.535
VIII	230	1.066	132	98	0.010	0.790	0.214	19.61	10.28	0.212	0.038*	0.900*	0.062

Note. Treatment: (I) suspending-drying; (II) suspending with PVA (15 wt.%) and drying; (III) MCA of dry powder with PVA (15 wt.%); (IV) MCA of dry powder with PVA, adsorption of water from saturated vapour and drying; (V) MCA of dry powder with PVA, adsorption of ethanol from saturated vapour and drying; (VI) MCA of oxides with PVA and 30 wt.% of water and drying; (VII) A-300 alone and (VIII) A-300/PVA, *c values for PVA contribution

Additionally (Table 1), PVP was bound to A–300 (content of isolated surface silanols C_{OH} ≈ 0.65 mmol/g, sample A-300(1)) at γ = 0.175 g/g using the PLS reactor. The adsorption of PVP was carried onto the preheated silica powder. The silica powder was loaded in the PLS reactor, then the PVP powder was added and the mixture was agitated for 0.5 h. Then ethanol (30 wt. % with respect to the silica weight) was dripped (one drop per second) in the reactor at room temperature and the mixture was agitated for 6 h, and then it was dried at room temperature. The samples were heated at 353 K for 2 h (Table 1, A–300/PVP(2)). Mixing of A–300/PVP(2) (30 g) with pure silica A–300(1) (20 g) in the PLSR for 0.5 h gives a sample A–300/PVP(3). The PLSR treatment of A–300/PVP(3) for 6 h in the presence of ethanol (30 wt. %) and drying at room temperature gives A–300/PVP(4). Then it was dried at 353 K for 2 h to prepare a sample A–300/PVP(5) (Table 1) [41].

The second set (Table 2), PVP was added to dry silica powder (then exposed in the saturated vapor of water or ethanol) or the aqueous suspension of silica, which then was treated in the ball mill during several hours. In another case, PVP was added to the aged aqueous suspension of silica. The textural characteristics of series of PVP/silica samples at different time of the MCA are shown in Table 2. The first sample is the initial A–300 heated at 723 K during several hours. Samples 2, 3, and 4 correspond to the MCA of dry A-300 for 1, 3, and 5 h, respectively. Samples 5, 6, and 7 are dry PVP/silica (γ = 0.1) after the MCA for 1, 3, and 5 h, respectively. Sample 8 is dry PVP/silica (γ = 0.2) after the MCA for 1 h. Sample 9 corresponds to Sample 8 dried after exposition in saturated vapor of water/ethanol (1:1) for 10 h. Samples 10, 11, and 12 correspond to dried powders with addition of 25 % solution of PVP in a mixture of ethanol and water (1:1) giving γ = 0.2 (the ratio between silica + PVP and water + ethanol is 2:1) after the MCA for 1–5 h [38–43].

The third set (Table 3), preparation of PVP/silica nanocomposites was carried out using two methods with (i) MCA and (ii) PLSR. In the first case, 25 g of silica (previously heated at 723 K for 3–4 h) was loaded into the ball mill and treated at room temperature. Amounts of added water, alcohol, and PVP and the activation time (t_{act}) are shown in Table 3. Then ball-milled samples were air-cured for 12 h and heated at 343 K for 2 h. In the case of the PLSR treatment, 25 g of silica loaded into the reactor was agitated at room temperature for 30 min. Then a given solution of PVP was added by drops and mixed at room temperature for 0.5–9 h (the treatment time is shown in Table 3), and then samples were dried as described above[38–43].

Commercial poly(vinyl alcohol) (PO "Stirol", Severodonetsk, Ukraine; molecular weight 43±7 kDa) was used as received (Tables 4 and 5). Various techniques were used to prepare oxide samples and PVA/silica nanocomposites (Table 4) [43–45]: (I) suspending-drying of nanosilicas; (II) suspending of oxides with PVA (monolayer loading) and drying; (III) mechanochemical activation of dry oxide powder with PVA in the ball-mill; (IV) MCA of dry oxide powder with PVA, adsorption of water from saturated vapour, aging for 24 h and drying; (V) MCA of dry oxide powder with PVA, adsorption of ethanol from saturated vapour, aging for 24 h and drying; and (VI) MCA of oxides with PVA and 30 wt. % of water and drying (Table 4). The PVA/oxide powders were also prepared by MCA suspending and drying of their mixtures at room temperature for 72 h and at 333 K for several hours at C_{PVA} = 9.1 and 16.7 wt. % with respect to silica (Table 5). The adsorption of PVA onto fumed oxides was carried out from distilled water and measured using a viscosimetry method. The adsorption was determined using a calibrating graph from the difference in the flow velocity of the PVA solution in a glass capillary before and after the adsorption (solid residue with adsorbed PVA was removed by centrifugation) at pH 6.3±0.2 and T = 298±2 K. Three measurements were performed for each adsorption point, and the average errors were smaller than ±5 % [43–45].

Poly(ethylene oxide), PEO (Sigma, MW ≈ 600 kDa) was used in the adsorption experiments [43, 46]. Samples of PEO/silica (Table 6) were prepared with a dried solid residual (after the PEO adsorption onto fumed silica in the aqueous medium, sample centrifugation and subsequent drying at room temperature and then at 343–393 K). Note that distribution of PEO at a surface of nanosilica using restricted amounts (≈ 30 wt. %) of solvents (water or alcohol) was unsuccessful due to the visco-mechanical properties of long PEO at MW = 600 kDa.

Table 5. Characteristics of A-300 alone and modified by PVA suspended and dried

C_{PVA} (wt.%)	S_{BET} (m^2/g)	V_p (cm^3/g)	S_{meso} (m^2/g)	S_{macro} (m^2/g)	V_{nano} (cm^3/g)	V_{meso} (cm^3/g)	V_{macro} (cm^3/g)	$<R_V>$ (nm)	$<R_S>$ (nm)	Δw	c_{void}	c_{cyl}	c_{void}
0	189	1.766	60	129	0.013	0.719	1.035	29.80	18.53	0.160	0.175	0.703	0.122
1.5	229	1.439	133	96	0.018	0.854	0.568	24.07	11.10	-0.027	0.001*	0.880*	0.119
7.0	178	1.353	67	111	0.006	0.913	0.434	21.91	12.94	-0.074	0.048*	0.921*	0.031
9.1	154	1.434	68	86	0.002	0.135	1.297	51.33	26.43	-0.379	0.491*	0.205*	0.304
13.0	140	1.105	50	90	0.007	0.586	0.512	25.98	13.13	-0.047	0.048*	0.770*	0.182
16.7	149	1.070	84	65	0.008	0.266	0.796	38.21	14.97	0.274	0.120*	0.582*	0.297

Note. *c values for PVA contribution

Table 6. Characteristics of initial and PEO-modified fumed silica in aqueous media (dried and degassed before the nitrogen adsorption measurements)

Sample	C_{PEO} (g/g)	S_{BET} (m^2/g)	V_p (cm^3/g)	S_{meso} (m^2/g)	S_{macro} (m^2/g)	V_{nano} (cm^3/g)	V_{meso} (cm^3/g)	V_{macro} (cm^3/g)	$<R_V>$ (nm)	$<R_S>$ (nm)	Δw	c_{void}	c_{cyl}	c_{void}
A-300	0	316	1.412	237	79	0.033	1.133	0.246	18.46	9.15	0.145	0.007	0.834	0.159
2	0.01	303	1.412	225	78	0.027	1.080	0.305	19.57	8.25	-0.025	0.017*	0.880*	0.103
3	0.02	282	1.331	209	73	0.026	0.994	0.311	20.01	8.09	-0.028	0.003*	0.792*	0.205
4	0.04	273	1.509	183	90	0.024	1.162	0.322	20.12	9.02	-0.101	0.003*	0.877*	0.120
5	0.08	259	1.547	165	94	0.025	1.060	0.462	21.80	9.43	-0.093	0.114*	0.756*	0.130
6	0.12	222	1.414	132	90	0.029	1.042	0.344	20.63	8.77	-0.266	0*	0.976*	0.024
7	0.16	192	1.213	120	72	0.023	0.770	0.347	22.77	9.23	-0.162	0.116*	0.759*	0.124
8	0.20	176	1.181	105	71	0.021	0.642	0.340	22.74	9.37	-0.217	0.067*	0.824*	0.109

Note. **c* values for PEO contribution

Table 7. Characteristics of initial and PEG (0.18 g/g, monolayer) modified fumed silica A-380

Sample	S_{BET} (m^2/g)	V_p (cm^3/g)	S_{meso} (m^2/g)	S_{macro} (m^2/g)	V_{nano} (cm^3/g)	V_{meso} (cm^3/g)	V_{macro} (cm^3/g)	$<R_V>$ (nm)	$<R_S>$ (nm)	Δw	c_{void}	c_{cyl}	c_{void}
A-380[s]	268	1.482	176	92	0.021	0.809	0.652	24.82	12.85	0.360	0.083	0.704	0.213
2[s]	164	1.555	51	113	0.009	0.780	0.766	27.28	14.21	-0.120	0*	0.954*	0.056
3[d]	177	0.828	127	50	0.017	0.431	0.381	25.41	8.93	0.099	0.031*	0.750*	0.219
4[wv]	169	0.578	142	27	0.020	0.362	0.196	23.54	6.64	0.128	0.002*	0.715*	0.283
5[av]	163	0.788	117	46	0.015	0.400	0.372	26.15	9.25	0.091	0*	0.780*	0.220
6[b]	165	0.739	132	33	0.017	0.467	0.255	25.70	7.86	0.055	0.248*	0.632*	0.120

Note. MCA treated (1 h) [s]suspension, [d]dry powder, [wv]water vapor, [av]ethanol vapor, [b]30 wt.% water;**c* values for PEG contribution at the pore walls

Therefore, the PEO adsorption on fumed silica A–300 was carried out in the aqueous medium. Measurements of the PEO adsorption was performed at varied initial C_{PEO} and a constant amount of fumed silica A–300 in the aqueous suspension (C_{SiO2} = 1 wt. %) at room temperature. The aqueous suspension of the silica with a given amount of dissolved PEO was stirred for 1 h. Then it was centrifuged at 8000 rpm for 30 min. The solid residue was dried at room temperature then at 373–393 K. Comparison of the PEO adsorption occurred for 1 h and 24 h showed near the same adsorption values. Therefore, the adsorption values were measured after the adsorption for 1 h. The PEO concentration in the liquid residue was determined interferometrically (from interferential diagrams for a pure solvent and given noncolored solutions of the studied solute in this solvent) using an ITR-2 (LOMO) interferometer. This apparatus provides the measurement accuracy of the index of refraction n_D^t up to $\pm 4\times10^{-6}$ which allows one to study both concentrated and diluted solutions of polymers [46].

Commercial poly(ethylene glycol), PEG (Fluka, 35 kDa) (Tables 7 and 8) was used as received. The interaction of PEG with fumed silica was previously described [43]. Several preparations of the silica/polymer powders were used: (i) ball-milling of dry mixtures of polymer and silica powders for 1 h; (ii) treatment of similar mixtures in saturated vapors of water or ethanol for 24 h followed by ball-milling for 1 h and drying; (iii) addition of 30 wt. % of water or ethanol to the treated dry silica/polymer powders; (iv) adsorption of polymers from aqueous solution, centrifugation and drying of the residual solid. Similar treatments were used to prepare nanosilica alone. Before the nitrogen adsorption/desorption measurements, silica samples were heated at 200 °C, but oxide/polymer materials were heated at 80 °C for 2 h [43].

Commercial polydimethylsiloxanes PDMS200 (label P1, viscosity of *ca*. 200 mm²/s, Table 9), PDMS1000 (P2, viscosity of *ca*. 1000 mm²/s) (“Kremniypolymer”, Zaporozhye, Ukraine), and PDMS12500 (P3) (Wacker® AK 12500 silicone fluid, purity > 99 %, viscosity of *ca*. 12500 mm²/s at 25 °C, density of *ca*. 0.97 g/cm³) were used for A–300 modification and preparation of composites (Table 9) [33, 34]. A series of modified silicas with the same content (16.7 wt. %) of chemically bound different PDMS was synthesized (in a glass reactor, volume 1 dm^3, with a mixer, 500 rpm) with the presence of dimethyl carbonate (DMC (label D), purity > 99.0 wt. %, as a siloxane bond breaking reagent, which does not contribute the weight of modified silica due to the reaction mechanism) in the gaseous dispersion media (*i.e.,* without a solvent) at 100 or 200 °C (using 10 g A–300, 2 g PDMS, and 2 g DMC). Upon the second stage, P3 (dissolved in *n*-hexane, purity > 99.9 %) was physically adsorbed (in the amount of 14–95 wt. %) onto unmodified or PDMS/DMC modified silicas (PDMS was rather filled by modified silica at C_{P3} > 50 wt. %). Before the PDMS adsorption, the samples were dried at 100 °C for 1 h, and then the *n*-hexane solution (3 wt. %) of P3 was added and the suspension was carefully stirred. It was dried at room temperature for 24 h and then at 100 °C for 3 h [33, 34].

Commercial polymethylsiloxane (PMS) hydrogel, synthesized using methyltrichlorosilane as a precursor, at ~ 7–8 wt. % of PMS and 93–92 wt. % of water (Enterosgel, Kreoma-Pharm, Ukraine) was used as an initial material (Table 10) [35–37]. After drying at room temperature for a week, the amount of water bound in PMS was small (0.7 wt. %). Dried and stirred PMS was rehydrated (h = 1 g/g) and stirred again. The bulk density of hydro-compacted wetted PMS powder is $\rho_b \approx 0.5$ g/cm^3 at $V_{em} \approx 1.5$ cm^3/g; *i.e.*, it remains as a disperse material, as well the blends with nanosilica (Table 8).

Samples of dry PMS and A–300 were mixed in a porcelain mortar, and then distilled water (h = 1 g/g) was added. If the system was stirred without any strong mechanical loading (simple mixing) that $\rho_b \approx 0.5$ g/cm^3 (PMS/A–300). If the system was stirred under strong mechanical loading (careful grinding in a porcelain mortar with strong hand-loading giving ~ 20 atm, estimated from the geometry of the mortar and a pestle used and a loading weight, for 15 min) that $\rho_b \approx 0.6$ g/cm^3. This is a hydro-compacted sample labeled as cPMS/A–300. Hydro-compaction of a set of nanomaterials based on unmodified and modified nanooxides was described in detail elsewhere [35–37, 57–62].

Table 8. Characteristics of initial and PEG (0.125 g/g, monolayer) modified fumed silica A-300

Sample	S_{BET} (m^2/g)	V_p (cm^3/g)	S_{meso} (m^2/g)	S_{macro} (m^2/g)	V_{nano} (cm^3/g)	V_{meso} (cm^3/g)	V_{macro} (cm^3/g)	$<R_V>$ (nm)	$<R_S>$ (nm)	Δw	c_{void}	c_{cyl}	c_{void}
S1[s]	163	1.156	64	99	0.011	0.608	0.537	26.08	12.46	-0.145	0.003*	0.928*	0.069
S2[d]	172	1.097	100	72	0.011	0.508	0.578	28.23	12.13	0.107	0.199*	0.725*	0.076
S3[wv]	185	1.193	100	85	0.012	0.649	0.532	25.35	12.05	0.029	0.001*	0.874*	0.125
S4[av]	196	1.368	100	96	0.013	0.723	0.632	26.51	12.58	-0.010	0*	0.886*	0.114
S5[b]	157	1.026	92	65	0.014	0.440	0.572	29.18	11.37	0.066	0.269*	0.579*	0.152

Note. MCA treated (1 h) [s]suspension, [d]dry powder, [wv]water vapor, [av]ethanol vapor, [b]30 wt. % water; *c values for PEG contribution

Table 9. Characteristics of A-300 alone and modified by PDMS/DMC (VCV/SCR method)

Sample (filler)	Label	C_{P3} (wt.%)	S_{BET} (m^2/g)	V_p (cm^3/g)	S_{meso} (m^2/g)	S_{macro} (m^2/g)	V_{nano} (cm^3/g)	V_{meso} (cm^3/g)	V_{macro} (cm^3/g)	$<R_V>$ (nm)	$<R_S>$ (nm)	Δw	c_{void}	c_{cyl}	c_{void}
A-300	A	0	277	0.917	226	51	0.023	0.348	0.546	36.00	10.04	-0.245	0.175	0.609	0.216
A-300	AP3_14	14	171	1.269	82	89	0.009	0.232	1.028	45.26	15.28	0.376	0.551*	0.352*	0.097
A-300	AP3_20	20	144	0.842	83	61	0.010	0.242	0.589	39.25	11.10	0.203	0.199*	0.489*	0.312
A-300	AP3_40	40	82	0.507	45	37	0.008	0.093	0.406	44.03	10.60	-0.015	0.005*	0.737*	0.258
A-300/PDMS200/DMC	AP1D	0	165	0.686	122	43	0.016	0.291	0.379	33.06	7.78	0.193	0.236*	0.470*	0.294
A-300/PDMS200/DMC	AP1DP3_14	14	100	0.776	46	54	0.007	0.123	0.646	48.17	14.79	0.204	0.337*	0.501*	0.162
A-300/PDMS200/DMC	AP1DP3_20	20	94	0.782	38	56	0.008	0.193	0.582	39.31	12.57	-0.183	0.002*	0.937*	0.061
A-300/PDMS200/DMC	AP1DP3_30	30	76	0.631	37	39	0.003	0.108	0.521	50.22	15.66	0.103	0.022*	0.703*	0.275
A-300/PDMS200/DMC	AP1DP3_40	40	59	0.301	37	22	0.008	0.064	0.229	40.60	8.14	-0.119	0*	0.870*	0.130
A-300/PDMS1000/DMC	AP2D	0	172	0.603	136	36	0.029	0.330	0.245	25.38	5.32	-0.171	0*	0.903*	0.097
A-300/PDMS1000/DMC	AP2DP3_14	14	124	0.861	55	69	0.008	0.214	0.639	40.28	12.57	0.107	0.284*	0.578*	0.138
A-300/PDMS1000/DMC	AP2DP3_20	20	106	0.932	46	60	0.002	0.075	0.855	57.19	25.49	-0.382	0.770*	0.219*	0.011
A-300/PDMS1000/DMC	AP2DP3_30	30	64	0.604	28	36	0.005	0.104	0.495	52.96	15.78	-0.044	0*	0.754*	0.246
A-300/PDMS1000/DMC	AP2DP3_40	40	56	0.407	32	24	0.005	0.054	0.347	51.81	12.31	-0.024	0.019*	0.749	0.232
A-300/PDMS12500/DMC	AP3D	0	196	0.655	160	36	0.025	0.329	0.300	28.68	6.02	0.058	0.012*	0.693*	0.294
A-300/PDMS12500/DMC	AP3DP3_14	14	109	0.853	45	64	0.001	0.083	0.769	48.26	21.57	-0.361	0.708*	0.187*	0.105
A-300/PDMS12500/DMC	AP3DP3_20	20	99	0.739	42	57	0	0.039	0.700	52.56	27.68	-0.389	0.938*	0.027*	0.035
A-300/PDMS12500/DMC	AP3DP3_30	30	77	0.664	37	40	0.005	0.115	0.544	51.32	14.72	-0.023	0*	0.750*	0.250
A-300/PDMS12500/DMC	AP3DP3_40	40	60	0.314	38	22	0.007	0.069	0.239	44.35	8.72	0.054	0.001*	0.767*	0.232

Table 10. Characteristics of PMS alone and PMS/A-300

Sample	S_{BET} (m^2/g)	V_p (cm^3/g)	S_{meso} (m^2/g)	S_{macro} (m^2/g)	V_{nano} (cm^3/g)	V_{meso} (cm^3/g)	V_{macro} (cm^3/g)	$\langle R_V \rangle$ (nm)	$\langle R_S \rangle$ (nm)	Δw	c_{void}	c_{cyl}	c_{void}
PMS	507	1.320	454	53	0.024	1.153	0.142	11.35	4.51	0.003	0.001*	0.735*	0.264*
Stirred PMS	572	2.604	493	79	0.016	2.252	0.336	16.47	7.03	-0.013	0.002*	0.898*	0.100*
PMS/A-300	354	1.265	297	57	0.028	1.013	0.225	17.36	7.12	-0.039	0.033*	0.879*	0.088
cPMS/A-300	407	1.021	372	35	0.024	0.955	0.042	8.28	4.28	0.046	0.015*	0.878*	0.107
A-300	289	0.850	249	40	0.026	0.437	0.387	27.91	8.18	-0.262	0.078	0.874	0.048

Table 11. Characteristics of dried suspensions of silica alone and with bound proteins

Sorbate	C_a (wt.%)	S_{BET} (m^2/g)	V_p (cm^3/g)	S_{meso} (m^2/g)	S_{macro} (m^2/g)	V_{nano} (cm^3/g)	V_{meso} (cm^3/g)	V_{macro} (cm^3/g)	$\langle R_V \rangle$ (nm)	$\langle R_S \rangle$ (nm)	Δw	c_{void}	c_{cyl}	c_{void}
-	0	278	1.458	184	94	0.022	0.958	0.478	21.58	12.40	0.339	0.004	0.797	0.199
Albumin	17.2	178	1.172	89	89	0.015	0.645	0.512	25.37	11.62	0.044	0.002*	0.678*	0.320
Albumin	23.0	160	1.084	88	72	0.009	0.554	0.521	25.42	13.20	0.227	0.171*	0.505*	0.324
Albumin	27.6	141	0.951	78	63	0.009	0.503	0.438	24.98	12.50	0.145	0.138*	0.557*	0.305
Gelatin	21.1	145	1.002	78	67	0.008	0.526	0.468	25.25	13.48	0.225	0.129*	0.514*	0.357
Gelatin	31.3	125	0.877	45	80	0.009	0.487	0.381	25.84	12.65	0.046	0.018*	0.722*	0.259
-	0	220[s]	1.424	109	111	0.021	1.197	0.206	20.46	12.80	0.082	0.006	0.899	0.095
Ossein	3.1	221	0.718	193	28	0.021	0.597	0.100	14.80	5.37	-0.074	0.002*	0.829	0.169
Ossein	13.6	151	0.543	128	23	0.012	0.444	0.087	15.80	5.98	-0.070	0.084*	0.830*	0.086
Ossein	24.0	112	0.405	96	16	0.001	0.276	0.127	22.40	8.68	-0.410	0.653*	0.306*	0.041

Note. *c values for protein contribution, [s]suspension dried

Egg albumin (molecular weight ≈ 4.4×10^4), gelatin (molecular weight ≈ 3.5×10^5), ossein (Indar, Kyiv, 20–29 kDa), and ethanol were used as received. Adsorption of proteins (Table 11) was studied without strong oxide pretreatment and with no addition of the electrolyte buffer solution [47–53]. Silica (40 mg of oxide per 5 ml of protein solution or 1 g oxide per 125 ml of the solution) was added to protein solution (0.6 wt. %), agitated for 0.5 h and adsorption was measured after exposure for 1 h (enough to reach the plateau adsorption value) and the suspension was centrifuged at 6000 rpm for 15 min. The Biuret reactant (4 ml) was added to the obtained supernatant (1 ml). After agitating, the solution was exposed for 0.5 h, then its optical density was measured spectrophotometrically at λ = 540 nm to calculate the adsorbed amounts of proteins comparing with the initial protein solution. This method is described in detail elsewhere. Notice that dependence of the albumin adsorption onto fumed oxides on pH was studied previously. Protein/silica residual was dried at 313 K and degassed at 333 K for 2 h before nitrogen adsorption measurements [47–53].

NITROGEN ADSORPTION

The nitrogen adsorption (77.4 K) has been used to evaluate the accessible specific surface area (SSA, S_{BET}), pore volume (V_p), and pore size distributions (PSD) and related contributions of nano-, meso-, and macropores [47–49, 64]. The nitrogen adsorption-desorption isotherms (Micromeritics ASAP 2010, 2020, 2405N, or 2420 and Quantachrome Autosorb adsorption analyzers), recorded for samples degassed at 80–100 °C (with polymer and protein composites) or 150–200 °C (pure silicas) for several hours, could be used to compute the differential PSD $f_V(R) \sim dV_p/dR$ and $f_S(R) \sim dS/dR$ for nanopores at radius $R < 1$ nm, mesopores at 1 nm < R < 25 nm, and macropores at 25 nm < R < 100 nm using such methods as density functional theory (DFT) [65, 66] and non-local DFT (NLDFT) [67, 68]. Complex pore models with cylindrical (C) pores and voids (V) between spherical nanoparticles (VCV method) with the corresponding equation parameters for different phases (both V and C for polymers and V for silica in composites and VCV for pure silicas) [69]. The VCV method with a self-consistent regularization (SCR) procedure [66, 69] allows one to consider the presence of several phases since the parameters of several types of surfaces (*e.g.,* silica, polymers, *etc.*) could be simultaneously used with appropriate pore models for each component. The use of the SCR/VCV procedure gives information on contributions (weight coefficients) of different pore types and different components into the total porosity and SSA. As a whole, the model errors can remain upon the use of the VCV/SCR method because the texture of any adsorbent is not strongly ordered (pores can have very complex shapes) and affected by a surface roughness, *etc.* However, the VCV/SCR method reduces the systematic errors appearing upon the application of the firm software for complex materials. As a whole, the accuracy of the textural characteristics depends on several factors such as the errors in: (i) estimation of the characteristics of probe molecules (*e.g.*, occupied area for N_2 depends on the surface chemistry of adsorbents and it is equal to 0.162 nm^2 for basal planes of carbons and 0.137 nm^2 for silica); (ii) the pore models; and (iii) the solution of the integral equations describing adsorption [64–78]. The total errors could be estimated as ±10–15 % with a high level of the repeatability of the adsorption data. It should be noted that the errors caused by the inaccuracy of the used computation methods (using appropriate complex models of pores and adsorbent surfaces) are smaller than those caused by some inaccuracy of the measurement methods [69–74]. In the case of the equilibrium adsorption of polymers, the errors appear due to some inaccuracy in determination of fractions of non-adsorbed and adsorbed polymers using various spectroscopic and gravimetric methods. Typically, the relative errors increase with decreasing equilibrium concentrations of polymers in the solutions. However, in the adsorption ranges close to monolayer or greater, the errors could be smaller that ±5 % [1–4, 33–78].

For better view of the PSD at large R values, the differential PSD with respect to the pore volume $f_V(R) \sim dV/dR$, $\int f_V(R)dR \sim V_p$ could be recalculated to incremental PSD (IPSD) at $\Phi_V(R_i) = (f_V(R_{i+1}) + f_V(R_i))(R_{i+1} - R_i)/2$ at $\sum\Phi_V(R_i) = V_p$) as it was shown for various adsorbents [66, 69–74]. The PSD functions with respect to the SSA $f_S(R) = w(f_V(R) - V_p / R) / R$ are calculated using the formfactor for cylindrical pores w = 2 and 1.36 for voids between NPNP in

cubic aggregates. The $f_S(R)$ functions were used to compute the values of S_{nano}, S_{meso}, and S_{macro} (Table 1). The effective w_{ef} values for random NPNP aggregates $w_{ef} = (S_{BET} / V_p) \int R f_S(R) dR / \int f_V(R) dR$ were also used to estimate the S_{meso} and S_{macro} values by integration of $f_S(R) = w_{ef}(f_V(R) - V_p / R) / R$ (Tables 2–11).

RESULTS AND DISCUSSION

The textural characteristics of disperse adsorbents depend strongly on the particulate morphology and the presence of hierarchical structures (*e.g.*, NPNP, aggregates, agglomerates, and visible particles for fumed oxides) from nano- to macro-sizes in the powder materials [1–4, 8, 11, 64, 75–78]. The morphological and textural characteristics can determine the efficiency of many applications (both nanooxides and composites) [1–7, 23–32, 79–82]. However, these characteristics also affect the toxicity of nanomaterials [83] that is, however, minimal for fumed silica [63]. For porous adsorbents with characteristic shapes of pores (*e.g.*, slit-shaped or cylindrical), there is a simple relationship between the average pore sizes (d) and the S/V ratio $d = \alpha V_p / S_{BET}$ (where α is the pore shape formfactor) [11, 64]. For highly disperse adsorbents composed of NPNP of various sizes, the similar dependence is rather questionable due to the absence of pores of a certain fixed shape (*e.g.*, cylindrical or slit-shaped) since voids between NPNP, characterized by a certain particle size distribution, have random and complex shapes. However, for fumed silicas, there is a certain tendency of increasing pore volume with increasing SSA value (or decreasing NPNP sizes) [73, 74] (Fig. 1 *a*).

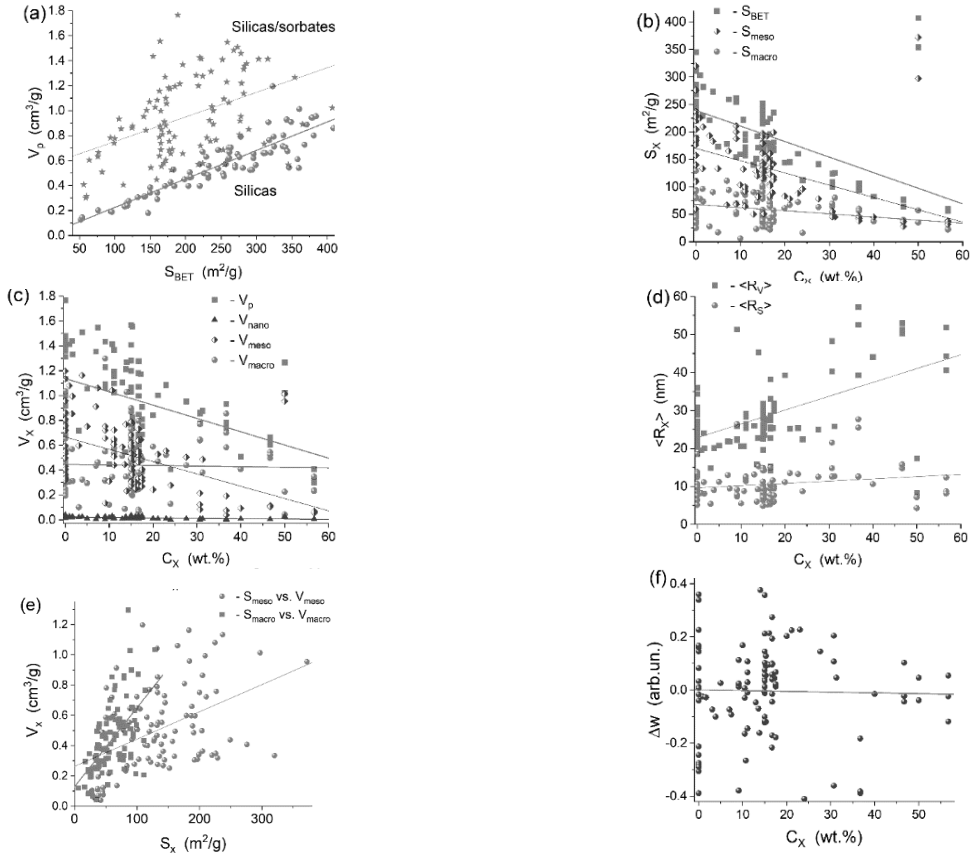

Fig. 1. Relationships between (*a*) the SSA and V_p values for fumed silicas alone (a set of samples of A–50, A–100, A–150, A–200, A–300, A–380, A–400) and A–300 and A–380 in various compositions with polymers and proteins with the similar ranges of the SSA values; (*b*) SSA and contributions of meso- and macropores, (*c*) V_p and nano-, meso-, and macropore contributions, (*d*) average pore radii with respect to the pore volume and SSA *vs*. sorbate content; (*e*) S_{meso} *vs*. V_{meso} and S_{macro} *vs*. V_{macro}; and (*f*) Δw *vs*. sorbate content. Pearson correlation coefficients for linear approximation is 0.89 for pristine silicas in (*a*), but for other cases, it is lower than 0.6, *i.e.*, the correlations are practically absent due to high scatters

This is due to enhanced aggregation of NPNP with decreasing their sizes. This tendency remains upon modification of nanosilicas by polymers or proteins if the systems remain porous (Fig. 1 *a*). However, the scatter becomes very high for the total set of the hybrid composites in comparison to pure nanosilicas with the SSA values in the same range. As a whole, the V_p values for the composites can be larger than that for pristine powder nanosilicas (Fig. 1 *a*). This effect is caused by several factors: (i) bulk density of composites or nanosilicas treated alone is greater than that of pristine silicas (V_{em} decreases) but V_p can increase because nitrogen adsorption efficiency increases; (ii) SSA value decreases (Fig. 1 *b*); (iii) a decrease in the distances between NPNP/polymer in the secondary and ternary structures (narrowing voids due to enhanced aggregation) results in an increase in contribution of narrower meso/macropores (Figs. 1 *c* and 2); (iv) the $<R_V>$ value can increase more strongly than $<R_S>$ (Fig. 1 *d*); (v) effective sizes of nanostructures with NPNP/polymer increase in comparison to pristine nanosilica; and (vi) the organization of the secondary and ternary structures changes, as well as the pore wall shapes. The presence of several different and sometimes opposite factors affecting the textural and morphological characteristics of all the composites studied causes a great scatter in the relationships between any pairs of the characteristics for the total set of samples (Fig. 1, Tables 1–11). However, stronger correlations could be found for each type of various composites (*vide infra*). Note that a contribution of nanopores (R < 1 nm) and narrow mesopores (1 nm < R < 3 nm) into porosity is small and depends weakly on the type and amounts of polymers/proteins in the composites (Figs. 2–11, Tables 1–11).

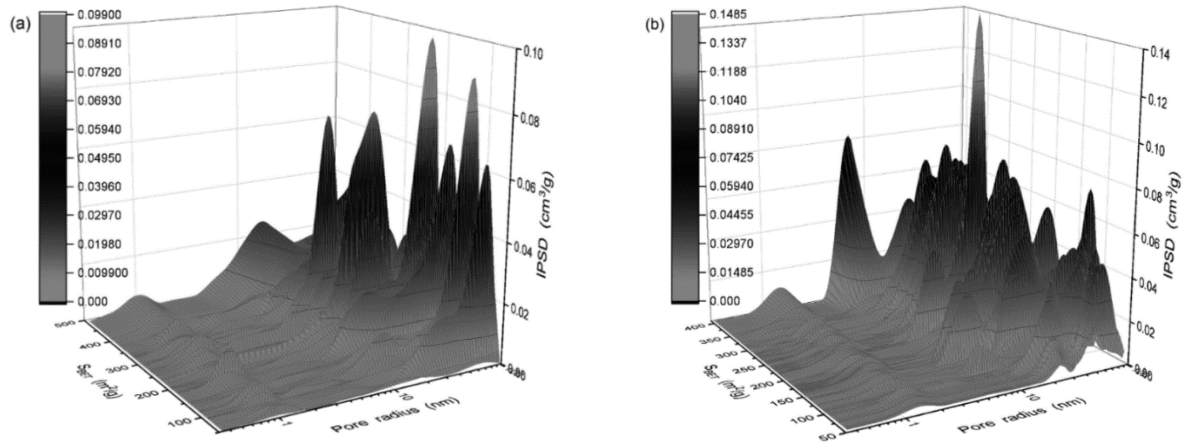

Fig. 2. DFT VCV/SCR IPSD for fumed silicas (*a*) alone and (*b*) in composition with polymers and proteins (samples are the same as in Fig. 1)

Features of the interactions of polymer – NPNP and polymer – polymer depend on the structure and numbers of active sites in the polymer chains and on NPNP surface. If the polymer sites are only electron-donor, electron-acceptor, and proton-acceptor ones (*e.g.*, C=O, C–O–C, C=N–C, Si–O–Si in PVP, PEO, PEG, PDMS, PMS) but non-proton-donor that the interactions with a silica surface should be stronger than that of polymer – polymer. If polymers (or proteins) include proton-donor, proton-acceptor and charged sites (*e.g.*, COH, COOH, COO^-, NH, NH^+, SiOH, *etc.*) that the interactions of adsorbates with silica NPNP (mainly with the SiOH groups) are characterized by similar energies as polymer - polymer (protein – protein) interactions [1–4, 8, 84–87]. Other factors such as co-adsorbates (*e.g.*, water, alcohol), temperature, concentrations, media characteristics, treatment conditions, *etc.* can also affect the structure of the whole composites and interfacial layers in the hybrid systems [1–10].

As a whole, the polymer composites can remain texturally porous, despite a certain decrease in the porosity and SSA values with increasing sorbate content (Tables 1–11). Therefore, 3D IPSD (DFT VCV/SCR) for nanosilicas alone is similar to that of the composites of nanosilicas with polymers and proteins (Fig. 2). However, there are some

differences caused by reasons mentioned above, especially by sorbate types, structures of polymer chains and active sites, and content that will be analyzed below.

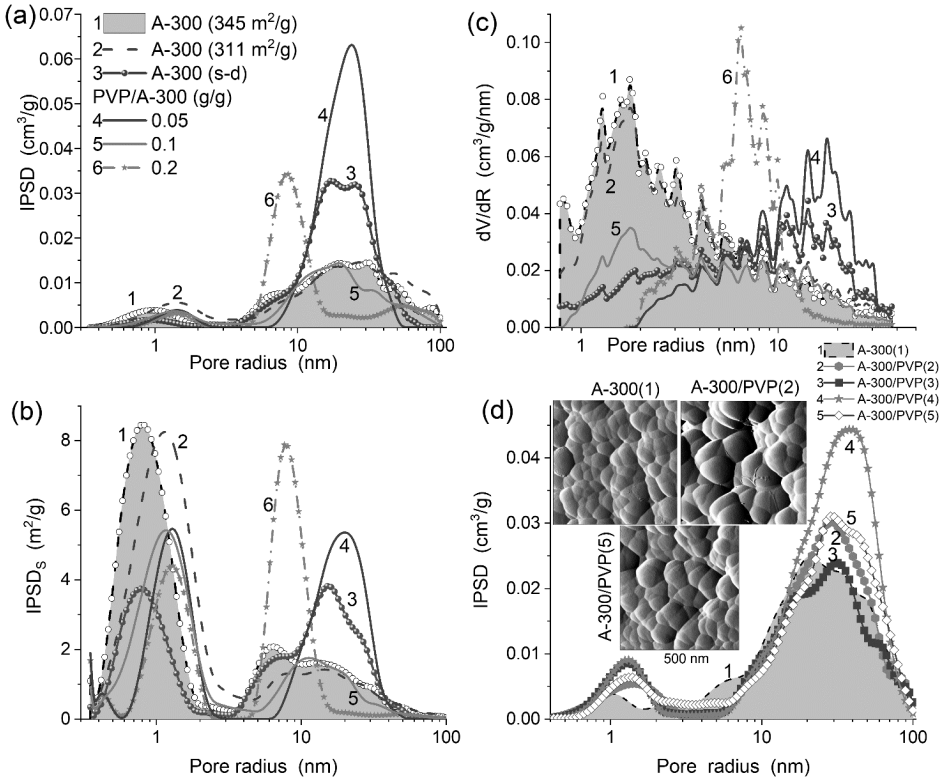

Fig. 3. Pore size distributions: DFT VCV/SCR IPSD with respect to (*a*) pore volume and (*b*) SSA, (*c*) differential NLDFT (model with cylindrical pores in silica) for A-300 alone and in composition with PVP; and (*d*) DFT VCV/SCR IPSD for A-300 (*1*) and A-300/PVP (*2–5*) (insert: AFM images of sizes 500×500 nm^2 [41]) (samples are shown in Table 1)

PVP interactions with silica nanoparticles and the textural organization of the composites depend on the PVP content (Table 1, Fig. 3), as well as on the MCA time and media characteristics (Tables 1–3, Figs. 3–5), affecting the amounts of silanol groups accessible for sorbates. An increase in the PVP content (C_{PVP}) and MCA time (t_{MCA}) leads to a decrease in the SSA values, but the V_p values demonstrate nonmonotonic changes. The main PSD peak of meso/macropores (Figs. 3–5, Tables 1–3, $S_{meso,macro}$, $V_{meso,macro}$) is typically shifted toward smaller pore sizes with increasing C_{PVP}. In general, the DFT VCV/SCR IPSD$_S$ functions with respect to SSA (Fig. 3 *b*) are similar to differential NLDFT (Fig. 3 *c*) with respect to mesopores. A large number of NLDFT PSD peaks (*i.e.*, dentate PSD curves) is due to a small value of the regularization parameter (fixed at too small value in Quantachrome software). Contribution of nanopores and narrow mesopores to the pore volume remains small, but it is larger for the SSA (comp. Figs. 3 *a*, *c* and 3 *b*). The main contribution into the PSD is caused by cylindrical pores with a polymer-covered surface of the pore walls (Tables 1–3, c_{cyl}). Note that PVP is used in medicine as an adhesive polymer. Its molecules, studied here, are relatively long (up to ~ 25 nm in length), and each linear PVP molecule can interact with several silica NPNP (< 10 nm in size). Therefore, the adhesive properties of PVP appear in shrinkage of the secondary structures of nanosilica (Fig. 4 clearly demonstrates this effect with shifted PSD peak *vs.* C_{PVP} and t_{MCA}). The average values of the pore sizes (Tables 1–3, $\langle R_V \rangle$ and $\langle R_S \rangle$ as the first moments of the distributions) show rather nonmonotonic changes. According to atom force microscopy images (Fig. 3 *d*, insert), enhanced treatments of the PVP/A–300+A–300 composite result in decreasing aggregates sizes and more uniform distribution of PVP with migration of a part of

macromolecules onto added fraction of A–300 [41]. All the textural and morphological changes in the PVP/A–300 composites are relatively complex because several factors can play an important role depending on the sorbate amounts, treatment time and other conditions. The complex morphology and topology of the composites reflect in changes in the pore model errors (Tables 1–3, Δw). Typically, treated nanosilicas alone are characterized by larger Δw values than composites. This is due to filling of interparticle voids by polymers; therefore, the pore walls become smoother and the Δw value (as a measure of surface roughness and random pore shapes) becomes smaller.

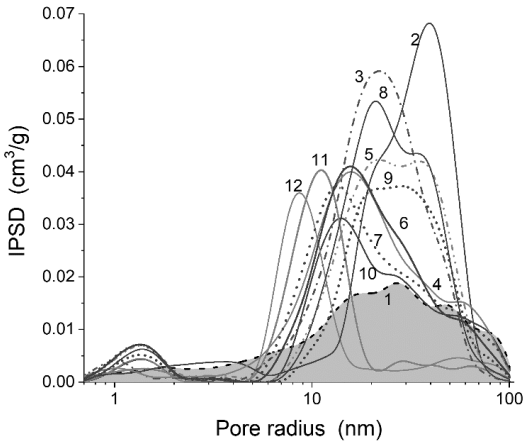

Fig. 4. Pore size distributions DFT VCV/SCR IPSD with respect to the pore volume for A-300 and PVP/A-300 samples shown in Table 2

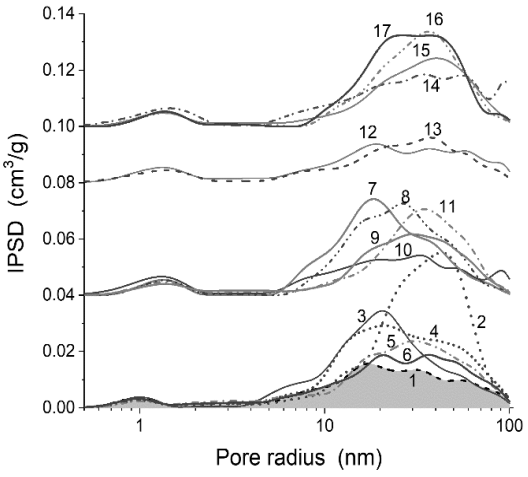

Fig. 5. Pore size distributions DFT VCV/SCR IPSD with respect to the pore volume for A-300 and PVP/A-300 samples shown in Table 3

Comparison of PVA having the proton-donor/proton-acceptor C–OH groups (Tables 4 and 5, Fig. 6) with PEO having much longer molecules (Fig. 7, Table 6) or PEG with molecules of similar length (Fig. 8, Tables 7 and 8) but having only proton-acceptor C–O–C groups shows that the PVA effects on the textural organization of the composites are rather similar to that of PVP since the PSD peak positions depend on C_{PVA} and treatment conditions. The adsorption of PEO and PEG can be rather considered as filling of large voids without so strong reorganization of the secondary and ternary structures of NPNP as by PVP or PVA. For the PEO/PEG composites, the PSD peaks (main contributions of cylindrical pores with the pore walls covered by polymers) do not shift but reduce the intensity with increasing polymer content in the composites.

Thus, PVP $(–CH_2CHR–)_n$, with the polar side groups R = NC_4H_6O and PVA $(–CH_2CHR–)_n$ with R = OH groups can more strongly interact with silica NPNP than PEO or PEG with the C–O–C bridges in the polymer chains $(–O–CH_2–CH_2–)_n$. However, PVP can be more easily distributed on the NPNP surfaces than PVA since the presence of the C–OH groups in PVA causes a tendency of the formation of tight polymer clews which are more poorly dissolved than PVP in the aqueous media. Therefore, according to the infrared spectra [43], the perturbation degree of free surface silanols of A–300 as a function of the polymer loading *vs*. C_{pol}/m_{seg} (where m_{seg} is the molecular weight of a segment) is similar for PEG, PEO, PVP, PDMS, and albumin but smaller for PVA. On the other hand, the composite durability and strength can be greater for PVA/A–300 than that for other systems studied here because of stronger binding –C(H)–OH– to ≡Si–OH and smaller steric effects in comparison to that for $–CH_2–O–CH_2–$ or $–Si(CH_3)_2–O–Si(CH_3)_2–$. This effect for the composites could be used to control the durability and dissolution rate of such water-soluble polymer films as PVA/starch/nanosilica.

For hydrophobic PDMS, there are the opposite effects with a certain shift of the PSD peaks toward larger pore sizes with C_{PDMS} (Fig. 9) than in the case of hydrophilic polymers (Figs. 3–8). This effect is confirmed by an increase in the values of $<R_V>$ and $<R_S>$ (Table 9).

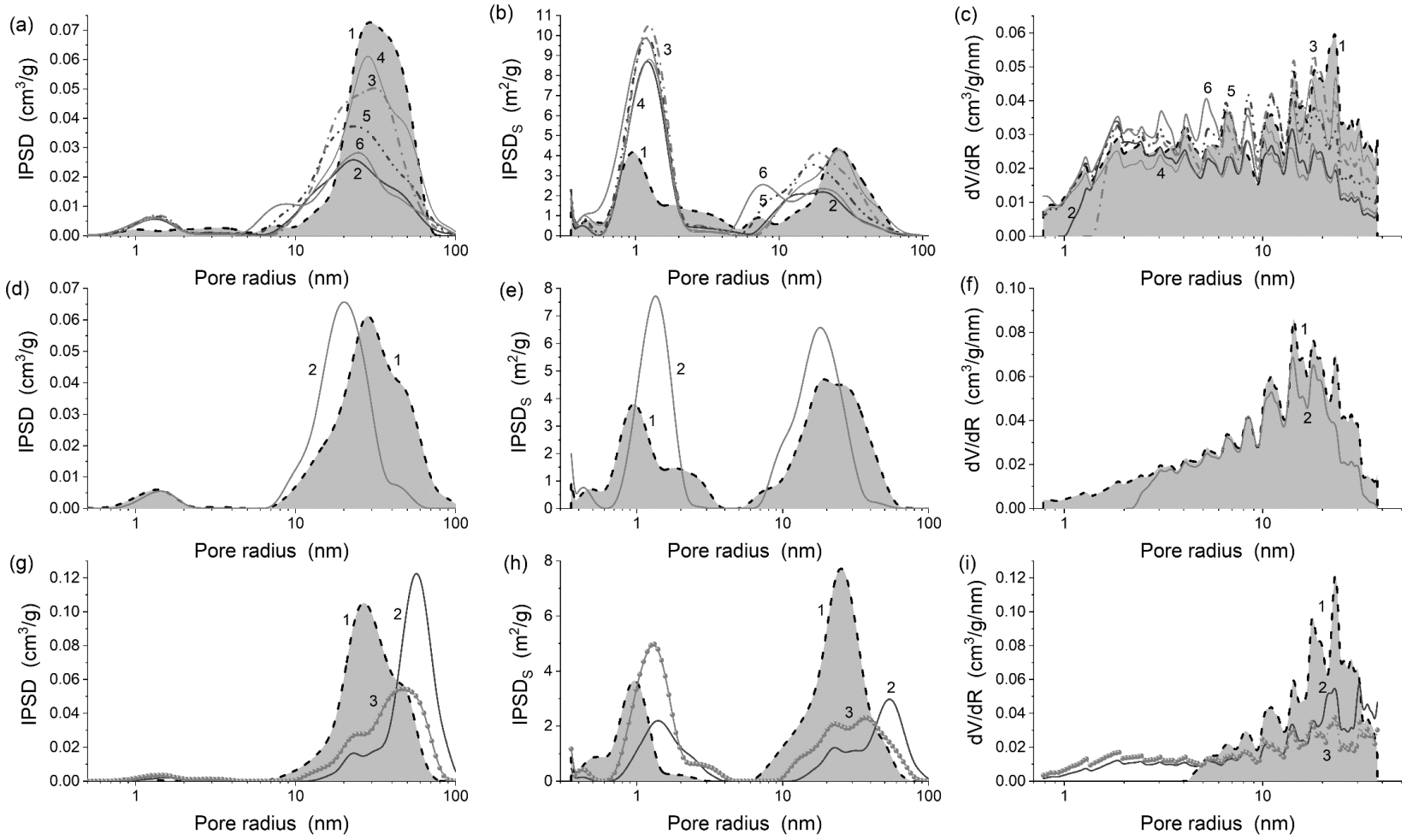

Fig. 6. Pore size distributions: DFT VCV/SCR IPSD with respect to (*a*, *d*, *g*) pore volume and (*b*, *e*, *h*) SSA and (*c*, *f*, *i*) differential NLDFT (model with cylindrical pores in silica) for A-300 alone and in composition with PVA (samples are shown in Table 4 (I-VI) for (*a–c*), (VII, VIII) for (*d–f*), and Table 5 (1.5, 7.0 and 13 wt. %) for (*g–i*), respectively)

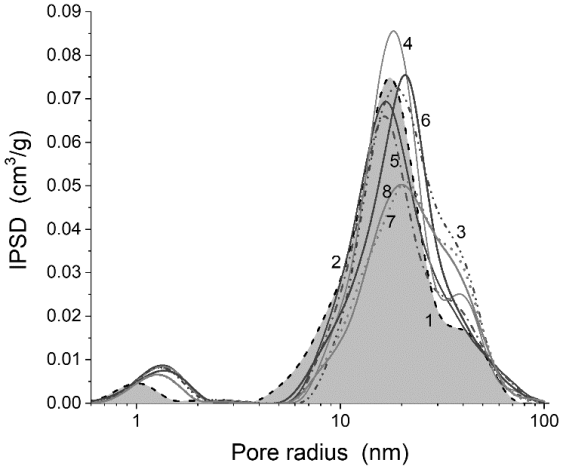

Fig. 7. Pore size distributions: DFT VCV/SCR IPSD with respect to pore volume for A-300 alone and with PEO (sample numbers correspond to them in Table 6)

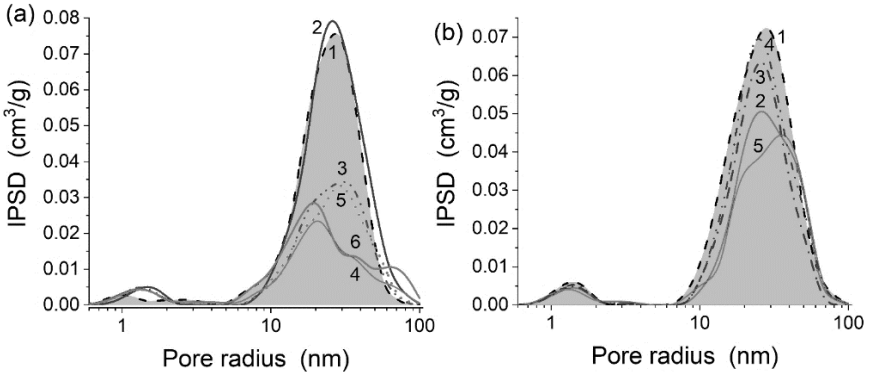

Fig. 8. Pore size distributions: DFT VCV/SCR IPSD with respect to pore volume for nanosilica alone and with PEG (sample numbers correspond to them in (a) Table 7 and (b) Table 8)

Additionally, in the case of PDMS, nanosilica chemically modified by PDMS/DMC (16.7 wt. %) was also adsorption modified with PDMS12500 (14–40 wt. %). Therefore, the double modification results in a strong diminution of the SSA and V_p values and an increase in contribution of macropores (Table 9, V_{macro}, S_{macro}, $<R_V>$). However, this diminution could be stronger if shorter PDMS (*e.g.*, PDMS200 or PDMS1000 instead of PDMS12500) is used as a modifier. A similar effect is observed during chemical modification of A–300 with PDMS/DMC and without adsorbed PDMS12500, *e.g.*, a diminution of the S_{BET} value becomes smaller with the molecular weight of PDMS (Table 9, S_{BET}, S_{meso}). This effect is due to steric barriers for location of longer coil PDMS chains in narrower voids. For the pore volumes, there is similar tendency but not so clear due to different reorganization of the secondary and ternary structures in composites and larger contribution of macropores (Table 9, V_{macro}) than mesopores (V_{meso}). Note that the pore model errors are minimal (Δw) at maximal amounts of PDMS in the composites and predominance of contribution of cylindrical pores with the pore walls with PDMS (Table 9, c_{cyl}*). The V_{nano} values are very small due to blocking of narrow voids by PDMS chemically and physically bound to the nanosilica surface.

In contrast to other studied polymers, PMS is 3D polymer with nanoclews bonded by certain bridges into 3D porous structures, which can be decomposed during MCA treatment [36, 37]. The SSA value of PMS is larger than that of A–300 with main contribution of mesopores (Table 10, Fig. 10). For the PMS/A–300 blends, the PSD peak shift depends strongly on the type of sample treatment because PMS is a relatively soft 3D polymer. The pretreatment with forced hydro-

compaction results in a stronger decrease in the pore sizes (PSD peak shits toward smaller sizes of pore radius) than for the composite with non-forced hydro-compaction demonstrating almost additive effect with respect to the PSD (Fig. 10, Table 10). This effect for the latter can be explained by the fact that for the PMS/A-300 blends, aggregates of nanoparticles of both types remain in the composite [36, 37].

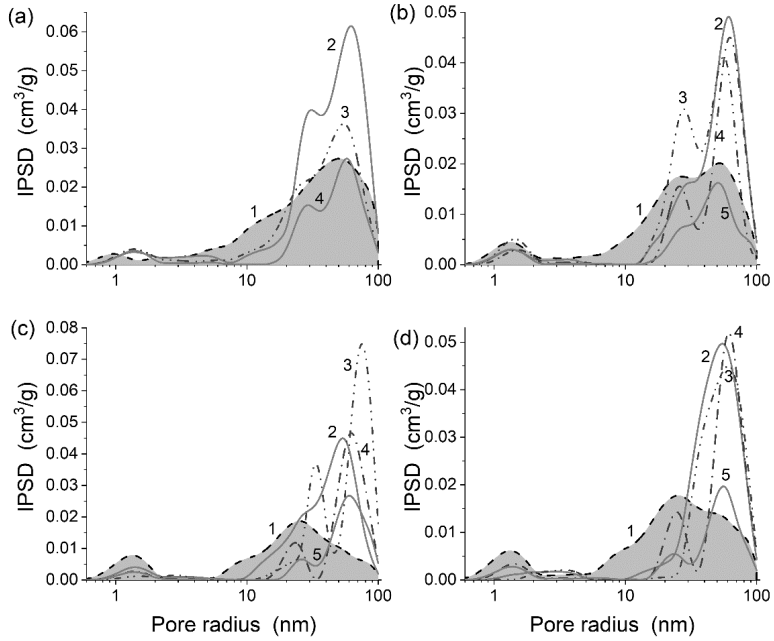

Fig. 9. Pore size distributions: DFT VCV/SCR IPSD with respect to pore volume for nanosilica alone and with PDMS (sample numbers correspond to them in Table 9 for four series of samples)

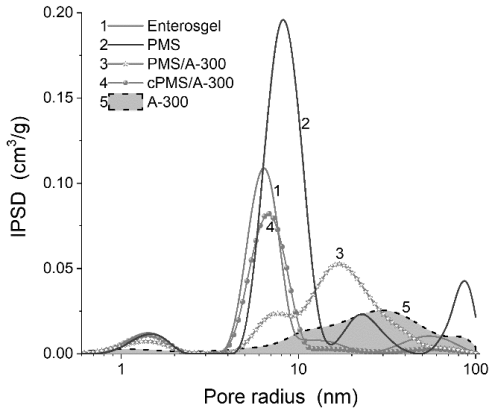

Fig. 10. Pore size distributions: DFT VCV/SCR IPSD with respect to pore volume for nanosilica and PMS alone and PMS/A-300 composites (samples correspond to Table 10)

For various proteins (Table 11, Fig. 11), characterized by strong intramolecular and intermolecular interactions, as well as by strong interactions with surface silanols, the textural changes in the composites depend on the molecular shape and size of such proteins as globular albumin and non-globular gelatin or ossein, protein content and other conditions. A maximal shift of the PSD peaks toward smaller pore sizes is observed for ossein (possessing minimal molecular weight among proteins studied) with a stronger diminution of the pore volume (Fig. 11, Table 11). Contributions of a protein surface into the values of weight coefficients are minimal for globular albumin (minimal PSD shift) and maximal for ossein

(Table 11, c*) with the maximal PSD shift (Fig. 11) and maximal pore filling (Table 11, V_p).

For egg albumin and gelatin, filling of large voids is stronger than the aggregate/agglomerate structure reorganization since the PSD peak shifts are not significant in the range of mesopores (Fig. 11 *a*) in contrast to ossein (Fig. 11 *d*). Changes in the $IPSD_S$ in the range of nanopores and narrow mesopores can be explained by narrow voids filling since the PSD intensity decreases (Fig. 11 *b*, *c*) with certain shift toward larger *R* values in comparison to A–300 alone, as well as own porosity of secondary protein structures.

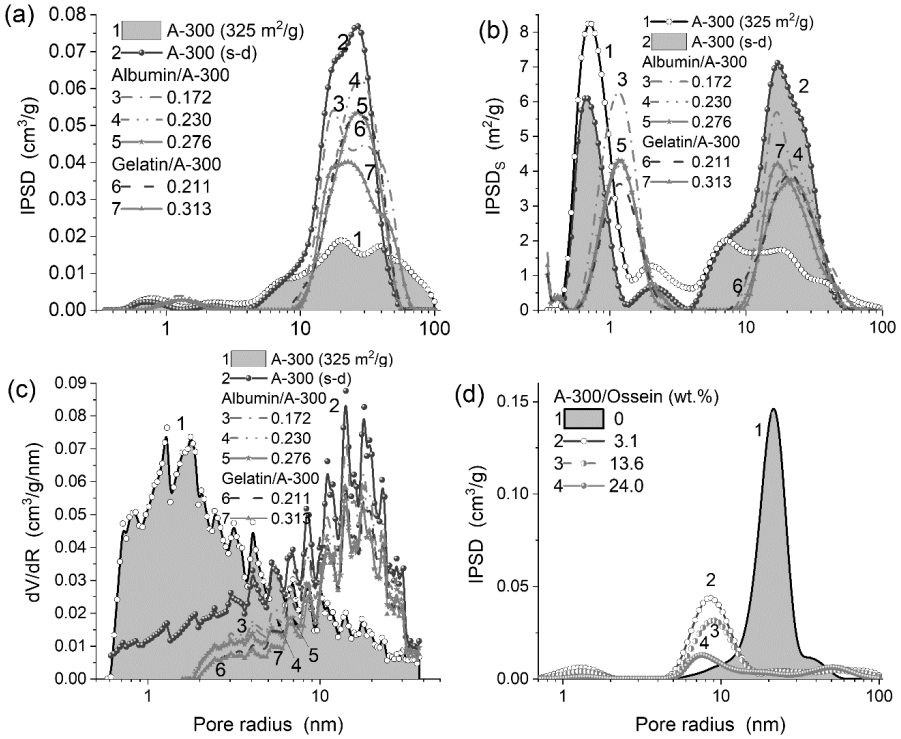

Fig. 11. Pore size distributions: (*a*, *b*, *d*) DFT VCV/SCR IPSD and (*c*) NLDFT with respect to (*a*, *c*, *d*) pore volume and (*b*) SSA for nanosilica alone and with proteins (samples correspond to Table 11)

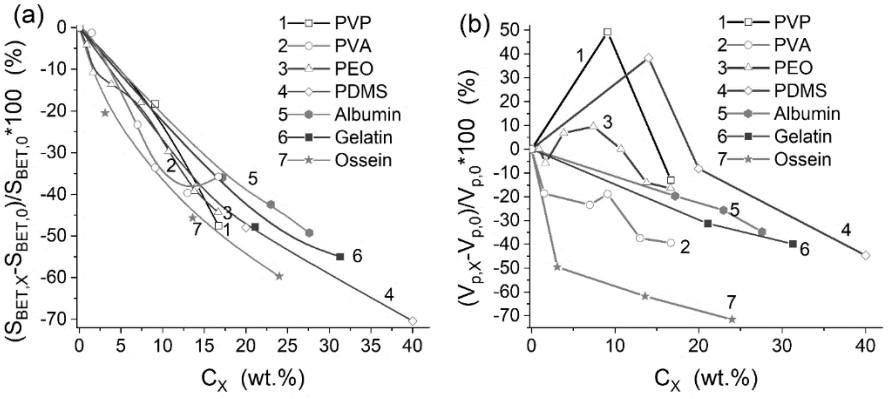

Fig. 12. Relative changes (%) in the (*a*) S_{BET} and (*b*) V_p values *vs*. content of sorbates for certain sets of samples

As a whole, the SSA loss dependent on the sorbate amounts is in similar courses for different compounds (Fig. 12 *a*). However, the difference in the SSA loss can reach up to 20 %, *e.g.*, for globular egg albumin macromolecules (Fig. 12 *a*, curve 5), remaining globular during adsorption, and smaller and non-globular ossein macromolecules (curve 7). PVA demonstrates

rather atypical curve because of enhanced PVA-PVA interactions with increasing sorbate amounts (Fig. 12 *a*). Relative changes in the V_p values are both positive and negative at C_X < 20 wt. % (Fig. 12 *b*) due to different reorganization of the hierarchical structures and occupation by adsorbed nitrogen only of a part of the empty volume since for highly disperse powders $V_p < V_{em}$. However, at $C_X > 20$ wt. %, only the loss of the pore volume is observed due to strong filling of voids by adsorbed macromolecules and compaction of the secondary and ternary structures.

CONCLUSION

The study of the textural and morphological characteristics of nanosilicas treated alone and in composites with PVP, PVA, PEO, PEG, PDMS, PMS, egg albumin, gelatin, and ossein shows that the reorganization of a set of hierarchical structures (aggregates of nanoparticles, agglomerates of aggregates, micro and visible particles), changes in the porosity and accessible surface area, contributions of pores of different sizes and shapes and with the pore walls with silica or polymer/protein depend on many factors. Among these factors, the type, molecular weight, and content of polymer/protein and treatment conditions play the main role. For total set of samples, the presence of a large set of factors results in strong scattering of the relationships for any pair of the textural characteristics or the amounts of sorbates and any textural characteristic. For narrow series of samples with the same silica and the same sorbate with only changes in the sorbate amount, there is stronger correlations for the SSA *vs*. C_X (since particle sizes increase due to adsorption of macromolecules) than that for the pore volume. This result is due to the textural organization features of highly disperse adsorbents characterized by a strong inequality $V_p << V_{em}$. The composite reorganization at all the structural hierarchy levels is strong but differently affects the V_p, V_{nano}, V_{meso}, V_{macro} and V_{em} values, but the inequality $V_p < V_{em}$ remains. However, the difference becomes smaller because the bulk density of any treated system with nanosilica increases and V_{em} decreases in comparison to the pristine powders. As a whole, selection of polymer, nanooxide, composition and certain conditions of the composite preparation allows one to control all the textural characteristics of the final material.

Developed VCV/SCR DFT method allows one to estimate not only the textural characteristics of complex systems but also to evaluate surface contributions of different phases in the nanocomposites with polymers or proteins and nanosilicas. Note that Quantachrome software (NLDFT) gives much worse PSD functions than VCV/SCR DFT due to several factors: (i) absence of the SCR procedure with estimation of contributions of different phases of samples studied; (ii) parameters of only one material which could be used (*e.g.*, silica or carbon); (iii) the regularization parameter is fixed and too small that results in generation of dentate PSD curves.

ACKNOWLEDGEMENTS

The work was supported by the National Research Foundation of Ukraine (Support of advanced and young scientists, grant 2020.02/0057). The author thanks Prof. V. Turov, Prof. E. Voronin, Dr. E. Pakhlov, Dr. L. Nosach, Dr. I. Protsak, Dr. L. Andriyko (Chuiko Institute of Surface Chemistry, Kyiv, Ukraine) for samples and Prof. Leboda R., Dr. Skubiszewska-Zięba J., Dr. B. Charmas, and Dr. D. Sternik (Maria Curie-Sklodowska University, Lublin, Poland) for nitrogen adsorption and microscopic measurements.

Текстурні характеристики та організація композитів із пірогенного кремнезему та високомолекулярних сполук

В.М. Гунько

Інститут хімії поверхні ім. О.О. Чуйка Національної академії наук України
вул. Генерала Наумова, 17, Київ, 03164, vlad_gunko@ukr.net

Різні композити з нанокремнеземом (та іншими нанооксидами) та полімерами мають практичне значення. Визначення детальних текстурно-морфологічних характеристик нанокремнеземів, оброблених окремо та в композитах з різними полімерами (лінійні полідиметилсилоксан, полівінілпірролідон, полівініловий спирт, поліетиленоксид та поліетиленгліколь, 3D-поліметилсилоксан) та білками (яєчний альбумін, желатин та осеїн) може розглядатися як інструмент для аналізу реорганізації ієрархічних структур у композитах (агрегати наночастинок, агломерати агрегатів, мікро- та видимі частинки). Цей аналіз дозволяє з'ясувати різні зміни пористості та доступної площі поверхні, внески пор різних розмірів, форм та стінок пор з кремнезему або полімера/білка залежно від різноманітних чинників. Зібрана інформація може бути використана для прогнозування можливих характеристик та властивостей різних композитів. Серед факторів, що впливають на властивості композитів, тип, молекулярна маса та вміст полімерів та умов тренування можуть відігравати головну роль. Наявність великого набору факторів ускладнює аналіз композитів, якщо використовувати спрощені підходи та методи. В цілому, вибір складу та певних умов створення композитів дозволяє контролювати всі текстурні характеристики кінцевих матеріалів, особливо, якщо всі вони точно оцінюються з мінімальними можливими помилками з використанням добре розвинених та адекватних методів.

***Ключові слова**: пірогенний кремнезем, полімери, білки, композити, морфологія частинок, текстурні характеристики*

REFERENCES

1. Iler R.K. *The Chemistry of Silica*: *Solubility, Polymerization, Colloid and Surface Properties and Biochemistry of Silica*. (Chichester: Wiley, 1979).
2. Legrand A.P. *The Surface Properties of Silicas*. (New York: Wiley, 1998).
3. Bergna H.E., Roberts W.O. *Colloidal Silica: Fundamentals and Applications*. (Boca Raton: CRC Press, 2006).
4. Somasundaran P. *Encyclopedia of Surface and Colloid Science*. Third Edition. (Boca Raton: CRC Press, 2015).
5. *Ullmann's Encyclopedia of Industrial Chemistry*. (Weinheim: Wiley-VCH, 2008).
6. Hastie J.W. *Materials Chemistry at High Temperatures.* V. 1. *Characterization.* V. 2. *Processing and Performance*. (Clifton NJ: Humana Press, 1990).
7. Büchel K.H., Moretto H.-H., Woditsch P. *Industrial inorganic chemistry*. (Weinheim: Wiley-VCHVerlag GmbH, 2000).
8. Gun'ko V.M., Turov V.V. *Nuclear Magnetic Resonance Studies of Interfacial Phenomena*. (Boca Raton: CRC Press, 2013).
9. Gun'ko V.M., Turov V.V., Zarko V.I., Goncharuk O.V., Pahklov E.M., Skubiszewska-Zięba J., Blitz J.P. Interfacial phenomena at a surface of individual and complex fumed Nanooxides. *Adv. Colloid Interface Sci*. 2016. **235**: 108.
10. *Basic characteristics of Aerosil fumed silica* (4th ed.). Tech. Bull. Fine Particles 11. (Hanau: Evonik Industries, 2014).
11. Adamson A.W., Gast A.P. *Physical Chemistry of Surface.* Sixth edition. (New York: Wiley, 1997).
12. Birdi K.S. *Handbook of Surface and Colloid Chemistry*. Third edition. (Boca Raton: CRC Press, 2009).
13. Al-Abadleh H.A., Grassian V.H. Oxide surfaces as environmental interfaces. *Surf. Sci. Report*. 2003. **52**(3–4): 63.
14. Barany S. *Role of Interfaces in Environmental Protection*. NATO Science Series IV Earth and Environmental Sciences. V. 24. (Dordrecht: Springer, 2003).
15. Nicolais L., Borzacchiello A., Lee S.M. *Wiley Encyclopedia of Composite. Materials*, 5-Volume set, 2nd ed. (Hoboken, NJ: Wiley, 2012).
16. Auner N., Weis J. *Oganosilicon Chemistry VI*. (Weinheim: Wiley-VCH Verlag GmbH, 2005).

17. Piemonte V., De Falco M., Basile A. *Sustainable Development in Chemical Engineering – Innovative Technologies. First Edition*. (Chichester, UK: John Wiley & Sons, 2013).
18. Theodore L., Kunz R.G. *Nanotechnology: Environmental Implications and Solutions*. (Hoboken, N.J.: John Wiley & Sons, 2005).
19. Hashim A.A. *Smart Nanoparticles Technology*. (Rijeka, Croatia: InTech, 2012).
20. *Cabot Corporation*. http://www.cabotcorp.com/solutions/products-plus/fumed-metal-oxides/
21. *DuPont*. http://www.dupont.com/.
22. *Evonik Ind*. http://corporate.evonik.com/en/Pages/default.aspx, http://www.aerosil.com/product/aerosil/en/services/downloads/Pages/test-methods.aspx
23. Ochsner A., Ahmed W., Ali N. *Nanocomposite Coatings and Nanocomposite Materials*. (Zurich: Trans Tech Publications Ltd, 2009).
24. Rahman R. *Silica and Clay Dispersed Polymer Nanocomposites. Preparation, Properties and Applications*. (Duxford: Elsevier, Woodhead Publishing, 2018).
25. Chung S.-C., Hahm W.-G., Im S.-S., Oh S.-G. Poly(ethylene terephthalate)(PET) nanocomposites filled with fumed silicas by melt compounding. *Macromol. Res*. 2002. **10**(4): 221.
26. Li Y., Yerian J.A., Khan S.A., Fedkiw P.S. Crosslinkable fumed silica-based nanocomposite electrolytes for rechargeable lithium batteries. *J. Power Sources*. 2006. **161**: 1288.
27. Rishi K., Pallerla L., Beaucage G., Tang A. Dispersion of surface-modified, aggregated, fumed silica in polymer nanocomposites. *J. Appl. Phys*. 2020. **127**(17): 174702.
28. Mora-Barrantes I., Rodríguez A., Ibarra L., González L., Valentín J.L. Overcoming the disadvantages of fumed silica as filler in elastomer composites. *J. Mater. Chem*. 2011. **21**(20): 7381.
29. Mahtabani A., Rytöluoto I., Anyszka R., He X., Saarimäki E., Lahti K., Paajanen M., Dierkes W., Blume A. On the Silica Surface Modification and Its Effect on Charge Trapping and Transport in PP-Based Dielectric Nanocomposites. *ACS Appl. Polym. Mater*. 2020. **2**(8): 3148.
30. Ver Meer M.A., Narasimhan B., Shanks B.H., Mallapragada S.K. Effect of mesoporosity on thermal and mechanical properties of polystyrene/silica composites. *ACS Appl. Mater. Interfaces*. 2010. **2**: 41.
31. Sipaut C.S., Adnan A.R., Rahman I.Ab., Bakar M.A., Ismail J., Chee C.K. Properties and morphology of bulk epoxy composites filled with modified fumed silica – epoxy nanocomposites. *J. Appl. Sci*. 2007. **7**: 27.
32. Sequeira D., Mascarenhas J., Picardo D., Dias R., Sutari O. Mechanical behaviour of fumed silica/glass reinforced polyester nanocomposites. *Am. J. Mater. Sci*. 2015. **5**(3C): 92.
33. Gun'ko V.M., Pakhlov E.M., Goncharuk O.V., Andriyko L.S., Nychiporuk Yu.M., Balakin D.Yu., Sternik D., Derylo-Marczewska A. Nanosilica modified by polydimethylsiloxane depolymerized and chemically bound to nanoparticles or physically bound to unmodified or modified surfaces: Structure and interfacial phenomena. *J. Colloid Interface Sci*. 2018. **529**: 273.
34. Gun'ko V.M., Turov V.V., Gorbik P.P. *Water at the Interfaces*. (Kyiv: Naukova Dumka, 2009).
35. Gun'ko V.M., Turov V.V., Zarko V.I., Goncharuk E.V., Gerashchenko I.I., Turova A.A., Mironyuk I.F., Leboda R., Skubiszewska-Zięba J., Janusz W. Comparative characterization of polymethylsiloxanehydrogel and silylated fumed silica and silicagel. *J. Colloid Interface Sci*. 2007. **308**(1): 142.
36. Gun'ko V.M., Turov V.V., Krupska T.V., Protsak I.S., Borysenko M.V., Pakhlov E.M. Polymethylsiloxane alone and in composition with nanosilica under various conditions. *J. Colloid Interface Sci.* 2019. **541**: 213.
37. Protsak I., Gun'ko V.M., Turov V.V., Krupska T.V., Pakhlov E.M., Zhang D., Dong W., Le Z. Nanostructured polymethylsiloxane/fumed silica blends. *Materials*. 2019. **12**(15): 2409.
38. Gun'ko V.M., Voronin E.F., Zarko V.I., Goncharuk E.V., Turov V.V., Pakhovchishin S.V., Pakhlov E.M., Guzenko N.V., Leboda R., Skubiszewska-Zięba J., Janusz W., Chibowski S., Chibowski E., Chuiko A.A. Interaction of poly(vinylpyrrolidone) with fumed silica in dry and wet powders and aqueous us pensions. *Colloids Surf. A*. 2004. **233**: 63.
39. Gun'ko V.M., Zarko V.I., Voronin E.F., Turov V.V., Mironyuk I.F., Gerashchenko I.I., Goncharuk E.V., Pakhlov E.M., Guzenko N.V., Leboda R., Skubiszewska-Zięba J., Janusz W., Chibowski S., Levchuk Yu.N., Klyueva A.V. Impact of some organics on structural and adsorptive characteristics of fumed silica in different media. *Langmuir*. 2002. **18**(3): 581.
40. Voronin E.F., Guzenko N.V., Gun'ko V.M., Malysheva M.L., Pakhlov E.M., Eremenko B.V., Chuiko A.A. Adsorption of polyvinylpyrrolidone and polyoxyethylene with pure and mixed silicon, aluminium, and titanium oxides. *Surface*. 2002. **7–8**: 5.
41. Gun'ko V.M., Voronin E.F., Nosach L.V., Pakhlov E.M., Guzenko N.V., Leboda R., Skubiszewska-Zięba J. Adsorption and migration of poly(vinyl pyrrolidone) at a fumed silica surface. *Adsort. Sci. Technol*. 2006. **24**: 143.

42. Gun'ko V.M., Voronin E.F., Nosach L.V., Pakhlov E.M., Voronina O.E., Guzenko N.V., Kazakova O.A., Leboda R., Skubiszewska-Zięba J. Nanocomposites with fumed silica/poly(vinylpyrrolidone) prepare data low content of solvents. *Appl. Surf. Sci.* 2006. **253**(11): 2801.
43. Gun'ko V.M., Leboda R., Skubiszewska-Zięba J., Goncharuk E.V., Nychiporuk Y.M., Zarko V.I., Blitz J.P. Influence of different treatments on characteristics of nanooxide powders alone or with adsorbed polar polymers or proteins. *Powder Technol*. 2008. **187**(2): 146.
44. Gun'ko V.M., Zarko V.I., Andriyko L.S., Leboda R., Skubiszewska-Zięba J., Janusz W. Interaction of nano oxides with poly(vinylalcohol). *Pol. J. Chem*. 2007. **81**(3): 411.
45. Gun'ko V.M., Pissis P., Spanoudaki A., Zarko V.I., Nychiporuk Y.M., Andriyko L.S., Goncharuk E.V., Leboda R., Skubiszewska-Zięba J., Osovskii V.D., Ptushinskii Y.G. Relaxation phenomena in poly(vinylalcohol)/fumed silica affected by interfacial water. *J. Colloid Interface Sci.* 2007. **312**(2): 201.
46. Voronin E.F., Gun'ko V.M., Guzenko N.V., Pakhlov E.M., Nosach L.V., Malysheva M.L., Skubiszewska-Zięba J., Leboda R., Borysenko M.V., Chuiko A.A. Interaction of poly(ethylene oxide) with fumed silica. *J. Colloid Interface Sci*. 2004. **279**(2): 326.
47. Gun'ko V.M., Zarko V.I., Goncharuk E.V., Andriyko L.S., Turov V.V., Nychiporuk Y.M., Leboda R., Skubiszewska-Zięba J., Gabchak A.L., Osovskii V.D., Ptushinskii Y.G., Yurchenko G.R., Mishchuk O.A., Gorbik P.P., Pissis P., Blitz J.P. TSDC spectroscopy of relaxational and interfacial phenomena. *Adv. Colloid Interface Sci*. 2007. **131**(1–2): 1.
48. Gun'ko V.M., Skubiszewska-Zięba J., Leboda R., Voronin E.F., Zarko V.I., Levitskaya S.I., Brei V.V., Guzenko N.V., Kazakova O.A., Seledets O., Janusz W., Chibowski S. Pyrocarbons prepared by carbonisation of polymers adsorbed or synthesised on a surface of silica and mixed oxides. *Appl. Surface Sci.* 2004. **227**(1–4): 219.
49. Gun'ko V.M., Zarko V.I., Voronin E.F., Goncharuk E.V., Andriyko L.S., Guzenko N.V., Nosach L.V., Janusz W. Successive interaction of pairs of soluble organics with nanosilica in aqueous media. *J. Colloid Interface Sci*. 2006. **300**(1): 20.
50. Blitz J.P., Gun'ko V.M. *Surface Chemistry in Biomedical and Environmental Science*. NATO Science Series II: Mathematics, Physics and Chemistry. V. 228. (Dordrecht: Springer, 2006).
51. Gun'ko V.M., Turov V.V., Leboda R., Zarko V.I., Skubiszewska-Zięba J., Charmas B. Adsorption, NMR and thermally stimulated depolarization current methods for comparative analysis of heterogeneous solid and soft materials. *Langmuir*. 2007. **23**(6): 3184.
52. Gun'ko V.M., Klyueva A.V., Levchuk Yu.N., Leboda R. Photon correlation spectroscopy investigations of proteins. *Adv. Colloid Interface Sci*. 2003. **105**(1–3): 201.
53. Gun'ko V.M. Competitive adsorption. *Theor. Exp. Chem.* 2007: **43**: 139.
54. Kulkarni P., Baron P.A., Willeke K. *Aerosol Measurement: Principles, Techniques, and Applications*. Third Edition. (New York: John Wiley & Sons, 2011).
55. Pietsch W. *Agglomeration in Industry*. (Weinheim: Wiley-VCH Verlag GmbH, 2005).
56. Biricik H., Sarier N. Comparative study of the characteristics of nano silica–, silica fume– and fly ash – incorporated cement mortars. *Mater. Res.* 2014. **17**(3): 570.
57. Gun'ko V.M., Turov V.V., Pakhlov E.M., Krupska T.V., Charmas B. Effect of water content on the characteristics of hydro-compacted nanosilica. *Appl. Surf. Sci.* 2018. **459**: 171.
58. Gun'ko V.M., Voronin E.F., Nosach L.V., Turov V.V., Wang Z., Vasilenko A.P., Leboda R., Skubiszewska-Zięba J., Janusz W., Mikhalovsky S.V. Structural, textural and adsorption characteristics of nanosilica mechanochemically activated in different media. *J. Colloid Interface Sci.* 2011. **355**(2): 300.
59. Gun'ko V.M., Zarko V.I., Leboda R., Chibowski E. Aqueous suspensions of fumed oxides: particle size distribution and zeta potential. *Adv. Colloid Interface Sci*. 2001. **91**(1): 1.
60. Gun'ko V.M., Turov V.V., Zarko V.I., Pakhlov E.M., Charmas B., Skubiszewska-Zięba J. Influence of structural organization of silicas on interfacial phenomena. *Colloids Surf A*. 2016. **492**: 230.
61. Gun'ko V.M., Mironyuk I.F., Zarko V.I., Turov V.V., Voronin E.F., Pakhlov E.M., Goncharuk E.V., Leboda R., Skubiszewska-Zięba J., Janusz W., Chibowski S., Levchuk Yu.N., Klyueva A.V. Fumed silicas possessing different morphology and hydrophilicity. *J. Colloid Interface Sci.* 2001. **242**(1): 90.
62. Gun'ko V.M., Voronin E.F., Mironyuk I.F., Leboda R., Skubiszewska-Zięba J., Pakhlov E.M., Guzenko N.V., Chuiko A.A. The effect of heat, adsorption and mechanochemical treatments on stuck structure and adsorption properties of fumed silicas. *Colloids Surf. A*. 2003. **218**: 125.
63. Younes M., Aggett P., Aguilar F., Crebelli R., Dusemund B., Filipic M., Frutos M.J., Galtier P., Gott D., Gundert-Remy U., Kuhnle G.G., Leblanc J.-C., Lillegaard I.T., Moldeus P., Mortensen A., Oskarsson A., Stankovic I., Waalkens-Berendsen I., Woutersen R.A., Wright M., Boon P., Chrysafidis D., Gurtler R., Mosesso P., Parent-Massin D., Tobback P., Kovalkovicova N., Rincon A.M., Tard A., Lambre C. Re-evaluation of silicon dioxide (E 551) as a food additive. *EFSA J*. 2018. **16**(1): 5088.

64. Gregg S.J., Sing K.S.W. *Adsorption, Surface Area and Porosity*. 2nd ed. (London: Academic Press, 1982).
65. Do D.D., Nguyen C., Do H.D. Characterization of micro-mesoporous carbon media. *Colloids Surf. A.* 2001. **187–188**: 51.
66. Gun'ko V.M. Textural characteristics of composite adsorbents analyzed with density functional theory and self-consistent regularization procedure. *Him. Fiz. Tehnol. Poverhni.* 2020. **11**(2): 163.
67. Ravikovitch P.I., Neimark A.V. Density functional theory model of adsorption on amorphous and microporous silica materials. *Langmuir.*2006. **22**(26): 11171.
68. Landers J., Gor G.Y., Neimark A.V. Density functional theory methods for characterization of porous materials. *Colloids Surf. A.* 2013. **437**: 3.
69. Gun'ko V.M. Composite materials: textural characteristics. *Appl. Surf. Sci.*2014. **307**: 444.
70. Gun'ko V.M. Various methods to describe the morphological and textural characteristics of various materials. *Him. Fiz. Tehnol. Poverhni.* 2018. **9**(4): 317.
71. Gun'ko V.M., Mikhalovsky S.V. Evaluation of slitlike porosity of carbon adsorbents. *Carbon.* 2004. **42**(4): 843.
72. Gun'ko V.M., Nano/meso/macroporous materials characterization affected by experimental conditions and features of the used methods. *Him. Fiz. Tehnol. Poverhni.* 2020. **11**(1): 5.
73. Gun'ko V.M. Morphological and textural features of various materials composed of porous or nonporous nanoparticles differently packed in secondary structures. *Appl. Surf. Sci.* 2021. **569**: 151117.
74. Gun'ko V.M. Features of the morphology and texture of silica and carbon adsorbents. *Surface*. 2021. **13(28)**: 127.
75. Gregg S.J., Sing K.S.W., Stoeckli H.F. *Characterization of Porous Solids*. (London: Soc. Chem. Industry, 1979).
76. Thommes M., Kaneko K., Neimark A.V., Olivier J.P., Rodriguez-Reinoso F., Rouquerol J., Sing K.S.W. Physorption of gases, with special reference to the evaluation of surface area and pore size distribution. IUPAC Technical Report. *Pure Application Chemistry.* 2015. **87**(9–10): 1051.
77. Lowell S., Shields J., Thomas M.A., Thommes M. *Characterization of Porous Solids and Powders: Surface Area, Porosity and Density*. (Dordrecht: Springer, 2004).
78. Rouquerol J., Baron G.V., Denoyel R., Giesche H., Groen J., Klobes P., Levitz P., Neimark A.V., Rigby S., Skudas R., Sing K., Thommes M., Unger K. The characterization of macroporous solids: An overview of the methodology. *Microporous. Mesoporous. Mater*. 2012. **154**: 2.
79. Kar K.K. *Composite Materials. Processing, Applications, Characterizations*. (Berlin: Springer, 2017).
80. Wilde G. *Nanostructured Materials*. (Amsterdam: Elsevier, 2009).
81. Reithmaier J.P., Petkov P., Wilhelm Kulisch W., Popov C. *Nanostructured Materials for Advanced Technological Applications*. (Dordrecht: Springer, 2009).
82. Kumar C.S.S.R. *Nanomaterials for the Life Sciences* V. 2. *Nanostructured Oxides*. (Weinheim: Wiley-VCH Verlag GmbH & Co., 2009).
83. Napierska D., Thomassen L.C.J., Lison D., Martens J.A., Hoet P.H. The Nanosilica Hazard: Another Variable Entity. *Part. Fibre Toxicol*. 2010. **7**: 39.
84. Zaia D.A.M. A review of adsorption of amino acids on minerals: Was it important for origin of life? *Amino Acids*. 2004. **27**(1): 113.
85. Hudson S., Cooney J., Magner E. Proteins in mesoporous silicates. *Angew. Chem. Int. Ed*. 2008. **47**(45): 8582.
86. Rimola, A., Costa D., Sodupe, M., Lambert J.-F., Ugliengo P. Silica surface features and their role in the adsorption of biomolecules: Computational modeling and experiments. *Chem. Rev.* 2013.**113**(6): 4216.
87. Kumar A.P., Depan D, Tomer N.S., Singh R.P. Nanoscale particles for polymer degradation and stabilization - Trends and future perspectives. *Prog. Polym. Sci*. 2009. **34**: 479.

Received 20.12.2021, accepted 01.06.2022